Acta Biomaterialia 185 (2024) 1–23

Contents lists available at ScienceDirect

Acta Biomaterialia

journal homepage: www.elsevier.com/locate/actbio

Review article

A comprehensive review on modeling aspects of infusion-based drug delivery in the brain

Tian Yuan[a,*], Wenbo Zhan[b], Michele Terzano[c], Gerhard A. Holzapfel[c,d], Daniele Dini[a,*]

[a] Department of Mechanical Engineering, Imperial College London, SW7 2AZ, UK
[b] School of Engineering, University of Aberdeen, Aberdeen, AB24 3UE, UK
[c] Institute of Biomechanics, Graz University of Technology, Austria
[d] Department of Structural Engineering, NTNU, Trondheim, Norway

ARTICLE INFO

Article history:
Received 21 March 2024
Revised 10 July 2024
Accepted 11 July 2024
Available online 19 July 2024

Keywords:
Brain disease
Computational modeling
Mechanical property
Drug delivery
Finite element method
Neuron
Biophysics
Biomechanics

ABSTRACT

Brain disorders represent an ever-increasing health challenge worldwide. While conventional drug therapies are less effective due to the presence of the blood-brain barrier, infusion-based methods of drug delivery to the brain represent a promising option. Since these methods are mechanically controlled and involve multiple physical phases ranging from the neural and molecular scales to the brain scale, highly efficient and precise delivery procedures can significantly benefit from a comprehensive understanding of drug-brain and device-brain interactions. Behind these interactions are principles of biophysics and biomechanics that can be described and captured using mathematical models. Although biomechanics and biophysics have received considerable attention, a comprehensive mechanistic model for modeling infusion-based drug delivery in the brain has yet to be developed. Therefore, this article reviews the state-of-the-art mechanistic studies that can support the development of next-generation models for infusion-based brain drug delivery from the perspective of fluid mechanics, solid mechanics, and mathematical modeling. The supporting techniques and database are also summarized to provide further insights. Finally, the challenges are highlighted and perspectives on future research directions are provided.

Statement of significance

Despite the immense potential of infusion-based drug delivery methods for bypassing the blood-brain barrier and efficiently delivering drugs to the brain, achieving optimal drug distribution remains a significant challenge. This is primarily due to our limited understanding of the complex interactions between drugs and the brain that are governed by principles of biophysics and biomechanics, and can be described using mathematical models. This article provides a comprehensive review of state-of-the-art mechanistic studies that can help to unravel the mechanism of drug transport in the brain across the scales, which underpins the development of next-generation models for infusion-based brain drug delivery. More broadly, this review will serve as a starting point for developing more effective treatments for brain diseases and mechanistic models that can be used to study other soft tissue and biomaterials.

1. Introduction

Neurological disorders, particularly brain diseases such as Alzheimer's disease, Parkinson's disease, brain tumors, epilepsy and stroke, represent a significant health challenge worldwide, especially given the rapid growth of the aging population over the last two decades [1]. The World Health Organization (WHO) estimates that neurological disorders will cause 12.22% of all deaths worldwide in 2030 [2]. Therefore, developing effective treatments for neurological disorders has been a major concern. While pharmacotherapy is a common treatment approach for various brain diseases, drug delivery to the brain is challenging due to the selective permeability of the blood-brain barrier (BBB). The BBB consists of closely connected endothelial cells and is additionally reinforced by astrocytes. It is a protective barrier

* Corresponding authors.
E-mail addresses: t.yuan19@imperial.ac.uk (T. Yuan), d.dini@imperial.ac.uk (D. Dini).

https://doi.org/10.1016/j.actbio.2024.07.015

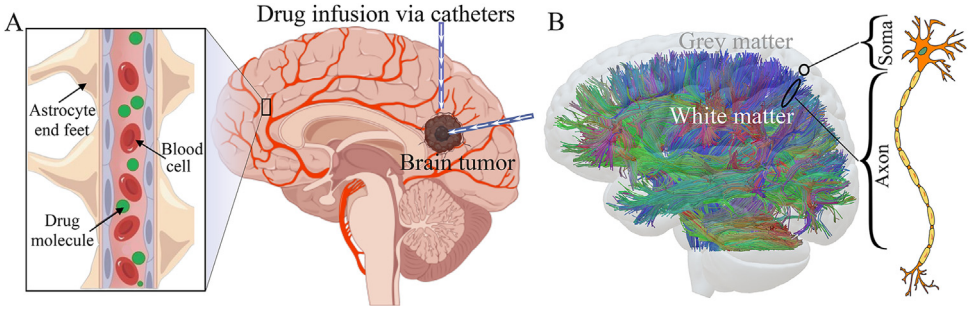

Fig. 1. Schematic representation of brain structures at different scales and the convection-enhanced delivery (CED) technique: (A) Schematic representation of the blood-brain barrier and the CED technique. (B) The color tracts are nerve fibers visualized by the diffusion tensor imaging technique. This shows the direction of nerve fibers in different regions. The nerve fibers (axons) form the white matter of the brain, while the cell bodies of the neurons (soma) form the brain gray matter.

that prevents harmful substances from entering the brain. This gives the BBB a selective function to properly transport nutrients, oxygen and metabolic wastes and filter the toxic substances, but along with most conventional drug molecules [3].

To penetrate the BBB and deliver drugs to the brain, some novel drug-delivery techniques have been developed. A promising approach is convection-enhanced delivery (CED) [4]. As schematically shown in Fig. 1A, CED involves the implantation of one or more catheters (or needles) into the brain to deliver the therapeutic agent to the target area by applying a pressure gradient, thereby physically bypassing the BBB [5]. Despite its high efficiency and accuracy, few desired results have been achieved in clinical CED trials for the treatment of brain diseases [6]. One of the biggest failures is the unwanted distribution of drugs, *e.g.*, some areas receive too little or too much of the drug [7], uneven distribution of drug concentration [8], backflow of the drug caused by incorrect pressure or catheter position [9], tissue damage caused by implantation of catheters [9]. Because it is a mechanically triggered and controlled drug delivery technique, these problems in CED could be alleviated by improving the current insufficient understanding of the fluid transport properties of the brain and the relationship of tissue response to local microstructural features and cells.

The brain is the most sophisticated soft tissue in nature, making it a source of endless scientific challenges. As shown in Fig. 1B, it is mainly composed of gray matter (GM) and white matter (WM). While GM consists of neuronal bodies and dendrites distributed on the surface of the brain to produce and process neuronal signals, WM contains bundles of nerve fibers or axons which transmit signals between neurons in different brain areas and between the brain and the rest of the body. Because the nerve fibers are enclosed by myelin, a sheath made of proteins and fat, the tissue appears relatively white and is therefore called white matter [10]. The nerve fibers connect different regions of the brain and have a specific orientation, giving WM a structural anisotropy. The combination of GM and WM, as well as the different packing patterns of neurons in different regions, make the brain tissue very heterogeneous. As drugs flow around neurons, the morphological features of brain tissue suggest that the micro-channel network for drug delivery is both anisotropic and heterogeneous. From a hydrodynamics perspective, this makes drug flow very complex and difficult to predict. In addition, since the neurons are extremely soft and the equivalent Young's modulus is in the range of $10^2 \sim 10^4$ Pa [11,12], the infused drug can easily deform the microstructure, which in turn changes the micro-channel network for drug delivery [13]. Since the diffusion of the drug molecules also depends on the shape of the micro-channels [14], the complex and deformable micro-channel network also makes the prediction of the diffusion efficiency (which can be characterized by the diffusion coefficient) challenging. Despite increasing research, the fundamental relationship between the flow status and the mechanical behavior of surrounding neurons is not yet clearly understood and defined. This unclear perception of the connection between fluid flow and neuron deformation may mislead clinical treatments at the brain level. Therefore, highly efficient drug delivery in the brain relies on (i) a clear and fundamental mechanistic understanding of how drug fluid and molecules are transported in brain tissue while interacting with them and (ii) a new model correlating microscale drug-neuron interactions with the macroscale drug transport properties of brain tissues, thus enabling accurate pre-operative predictions of the drug-delivery process in the brain.

Computational modeling plays an increasingly important role in understanding drug transport in the brain [15–19]. It can provide cost-effective approaches to (i) conduct comprehensive parametric sensitivity analyzes to identify the most influential factors; (ii) allow for individual examination multiple steps and factors involved in drug delivery, taking into account the effects of other steps and factors; and (iii) integrate clinically controllable parameters such as drug dose and administration schedule into *in silico* models. Once fully validated, the models can be used to assist in the design of drug delivery systems for optimal therapeutic responses [20]. This can also help reduce the number of laboratory and animal experiments. However, developing a comprehensive mathematical framework for brain drug delivery is challenging. First of all, it is important to correctly define the individual physical phases of the entire delivery process at the respective scales. The phases include the fluid phase (*e.g.*, drug fluid, interstitial fluid (ISF) and cerebrospinal fluid (CSF) [21,22]), the solid phase (*e.g.*, neurons [13,23] and tissues [24,25]), and the molecular phase (*e.g.*, drug molecules [26,27]). Second, the transport processes span large length and time scales, from the cellular and molecular scale (nm $\sim$ μm, μs $\sim$ s) [13,23,28], through the tissue scale (μm $\sim$ mm, ms $\sim$ min) [24,29], to the organ scale (cm, h $\sim$ day) [30–32]). Most importantly, these transport processes, which involve different phases and time/length scales, are usually strongly coupled.

Under these circumstances, an in-depth analysis of the mechanisms and theories of infusion-based drug delivery in the brain, as well as a comprehensive review of relevant recent studies are particularly important. This will not only help expand the currently insufficient knowledge of drug transport in the brain, but also improve our ability to accurately predict this process. From a physical point of view, the process of drug delivery in the brain is mainly governed by the interactions between the fluids (including the solutes, *e.g.*, drug molecules) and the solids, which take place at different scales. At the tissue level, interactions between the drug fluid and tissue opens gaps between the needle and the tissue, leading to local tissue swelling and backflow of the drug to the tissue surface. At the cellular level, interactions between the drug fluid and the cells alter the tissue microstructure, thus changing the flow pathway and tissue permeability; this controls the bipha-

sic property of the brain tissue and can be described by a poroelastic model at the tissue level. Capturing such a complex process requires a fundamental understanding and accurate mathematical descriptions of the key factors controlled by fluid mechanics and solid mechanics at the tissue and cellular levels. Fortunately, there are some comprehensive literature reviews that discuss the mechanical properties of the brain [33] and testing methods [34], the mechanics of the brain [35] and computational models for axonal cytoskeletal components of neuron [36], physiological mechanisms of fluid transport mechanism in the brain [37] and computational models of drug delivery to brain tumors. They have provided important insights into modeling the mechanical processes in the brain. However, there is still a gap in integrating the methods and techniques from different areas to build a comprehensive mathematical model to accurately predict the drug delivery process in the brain.

In order to close this gap, in this review article we first deal with fluid mechanics (Section 2) and solid mechanics (Section 3 at the tissue scale and Section 4 at the cellular scale) involved in infusion-based drug delivery in the brain. Note that the principle of fluid mechanics at the cellular level is primarily the Navier-Stokes (NS) equations. Therefore, in Section 2 we focus mainly on the principles of fluid mechanics at the tissue scale. Then, in Section 5, we provide an overview of the mathematical models that can integrate inputs obtained by applying fluid mechanics and solid mechanics methods to model the process of drug delivery throughout the brain. Finally, in Section 6, we summarize the key findings of the reviewed studies, analyze the limitations of current research, and propose strategies to close the research gaps. The insight provided in this review will serve as a starting point for the development of more comprehensive and accurate computational models that can accurately predict the brain drug delivery process, thereby improving the treatment efficiency of infusion-based brain drug delivery.

2. Fluid mechanics: fluid flow and mass transfer in the brain

From the perspective of fluid mechanics, drug delivery in the brain occurs primarily through (i) convection, *i.e.* transport by fluid flow, (ii) diffusion, *i.e.* transport through molecules' thermal motion, and (iii) reaction, *i.e.* the biochemical interactions between drug molecules and the other substances. The entire process can be briefly described by the convection-diffusion reaction equation [21]:

$$\frac{\partial(\phi C_n)}{\partial t}+\frac{\partial(\rho C_{Sn})}{\partial t}+\nabla\cdot\underbrace{(\boldsymbol{u}_F C_n)}_{\text{Convection}}=\nabla\cdot\underbrace{[(\mathbf{D}_n+\mathbf{D}_{Sn})\nabla C_n]}_{\text{Diffusion}}+\underbrace{R(C_n)}_{\text{Reaction}}, \tag{1}$$

where n denotes the species of drug particles, ϕ is the tissue porosity, C_n (mol/l) is the particle concentration in the fluid phase, C_{Sn} (mol/unit dry weight of the cells) is the amount absorbed by the cells, $\rho=(1-\phi)\rho_S$ is the dry bulk density and ρ_S is the cell density, t is time, $\mathbf{u}_F$ is the flow velocity, $\mathbf{D}_n$ (m^2/s) is the particle diffusion tensor in the fluid phase, $\mathbf{D}_{Sn}$ is that in the solid phase, $R(C_n)$ defines the biochemical reaction processes of the drug particles.

2.1. Convection

Driven by the fluid flow, the convection term in Eq. (1) can be obtained by solving the NS equations. However, because of its physiological structure, as shown in Fig. 1, brain tissues are widely treated as porous media. The NS equations must therefore be modified to take into account the effect of the porous medium on the drug delivery pathway, *i.e.*

$$\text{Continuity equation}\qquad \frac{\partial\rho_F}{\partial t}+\nabla\cdot(\rho_F\mathbf{u}_F)+\mathbf{S}=\mathbf{0}, \tag{2}$$

$$\text{Momentum equation}\qquad \rho_F\left(\frac{\partial\mathbf{u}_F}{\partial t}+(\mathbf{u}_F\cdot\nabla)\mathbf{u}_F\right)=-\nabla p+\mu_F\nabla^2\mathbf{u}_F+\rho_F\mathbf{f}, \tag{3}$$

where ρ_F is the fluid density, S is the source term counting for the plasma leakage (or fluid exchange between tissue and the blood lumen), p is the hydraulic pressure, μ_F (Pa · s) is the dynamic viscosity of the fluid and $\mathbf{f}$ is the force per unit volume that the porous medium exerts on the fluid.

The above equations are strongly coupled, nonlinear and have no analytical solutions. Therefore, Darcy's law, as a simplified version of the NS equations, is more widely used to determine the flow field in porous media. Named after Henry Darcy, a French engineer who first formulated it in 1856 based on the results of experiments on the flow of water through sand beds, Darcy's law expresses a proportional relationship between the pressure drop and the flow rate in porous media, described as

$$\mathbf{w}=-\frac{\boldsymbol{\kappa}}{\mu_F}\nabla p, \tag{4}$$

where $\mathbf{w}$ (m/s) is the averaged flow velocity over the cross section and $\boldsymbol{\kappa}$ (m^2) is the hydraulic permeability tensor of the porous medium, which measures the ability of the material to allow fluids to pass through. It is worth noting that in order to apply Darcy's law, the following conditions must be met:

(i) the fluid must be incompressible and Newtonian, *i.e.*, Eq. (2) can be reduced to $\nabla\cdot\mathbf{u}_F=0$;
(ii) the flow must be slow and steady so that the convective acceleration is small compared to the viscous forces, *i.e.*, Eq. (3) can be reduced to $\nabla p=\mu_F\nabla^2\mathbf{u}_F+\rho_F\mathbf{f}$;
(iii) the porous medium must be fully saturated and homogeneous so that the above equation can be further reduced to $\nabla p=\mu_F\nabla^2\mathbf{u}_F$ and a local volume-averaging approximation can be applied.

Although Darcy's law was originally obtained as an empirical expression based on experimental measurements, it can be derived theoretically by substituting the above assumptions into the NS equations [38–40]. This makes Darcy's Law a fundamental principle in the mechanics of porous fluids. Because of its universality, Darcy's law has numerous applications in various fields of science and engineering, including hydrogeological science, soil mechanics, petroleum engineering, environmental engineering, and biomedical engineering. The adoption of Darcy's law to model fluid transport in the brain, *e.g.*, to understand the formation and resolution of hydrocephalus and oedema, goes back to the 1980s [41,42]. In the past two decades, due to the sharp increase in the incidence rate of brain diseases, great attention has been paid to the development of highly efficient drug delivery techniques to cure brain diseases. Darcy's law is now more practically applied to predict and optimize the procedures of drug delivery to the brain, especially for direct and localized drug delivery methods in the brain, *e.g.*, CED [43,44].

Application of Darcy's law requires knowing the hydraulic permeability tensor $\boldsymbol{\kappa}$ of the target porous medium, which largely depends on the microstructure of the medium, *e.g.* pore size and distribution, and is usually characterized by measuring the flow rate in the samples under a given pressure drop [24,45].

Table 1 shows a summary of the characterized permeability of brain tissues. The methods developed for brain permeability characterization will be detailed in Section 2.4.1.

Table 1
Hydraulic permeability of brain tissue determined using various methods. The values correspond to the scalar components of isotropic or transversely isotropic permeability tensors.

Tissue type	Permeability κ (m^2)	Method	Refs.
Hepatic neoplastic tissue *in vitro*	3.1×10^{-17}	Lab test	[46]
Hepatic neoplastic tissue *in vivo*	$(2.9 \sim 8.4) \times 10^{-18}$	Lab test	[46]
MCaIV murine mammary carcinoma	1.86×10^{-15}	Lab test	[47]
LS174T human colon adenocarcinoma	3.37×10^{-16}	Lab test	[47]
U87 human glioblastoma	4.87×10^{-16}	Lab test	[47]
HSTS 26T human soft tissue sarcoma	6.9×10^{-17}	Lab test	[47]
Human brain tissue	2.47×10^{-17}	Lab test	[48]
Sheep corona radiata $\perp^*$	7×10^{-17}	Lab test	[24]
Sheep corona radiata $\parallel^{**}$	2×10^{-16}	Lab test	[24]
Sheep corpus callosum $\perp$	7.94×10^{-16}	CFD	[28]
Sheep corpus callosum $\parallel$	1.71×10^{-15}	CFD	[28]
Sheep fornix $\perp$	4.32×10^{-16}	CFD	[28]
Sheep fornix $\parallel$	9.05×10^{-16}	CFD	[28]
Sheep WM $\perp$	$(0.9 \sim 1.8) \times 10^{-16}$	Theory and CFD	[49]
Sheep WM $\parallel$	$(0.48 \sim 0.82) \times 10^{-16}$	Theory and CFD	[49]

* $\perp$: perpendicular to nerve fibers ** $\parallel$: parallel to nerve fibers.

2.2. Diffusion

The diffusion behavior of drug particles is determined by the thermal motion of the particles themselves and the effects from the liquid environment, cells and other substances. According to Fick's law [50], the fundamental principle that describes the diffusion of molecules, the rate of diffusion of a substance is proportional to the concentration gradient of the substance across the diffusion domain, *i.e.*

$$\mathbf{J} = -\mathbf{D}\nabla C, \tag{5}$$

where $\mathbf{J}$ is the diffusion flux vector, representing the amount of substance moving through a unit area per unit time, and ∇C is the concentration gradient of the diffusing substance, representing the concentration changes with position. The negative sign in the equation indicates that the substance diffuses from higher to a lower concentration. The coefficient $\mathbf{D}$ denotes the diffusion tensor, which determines the diffusion efficiency. Analogous to hydraulic permeability, the isotropic diffusion coefficient D of a specific particle in the brain microenvironment is a key parameter in determining the drug delivery route. It can be determined both through laboratory tests and numerical simulations, mainly based on Fick's law, i.e. Eq. (5), by measuring the flux and concentration gradients [51–54], and the Einstein diffusion Eq. (6), by recording the dynamics of the displacement of each individual particle. Thus, the diffusion coefficient D may be given as

$$D = \frac{\langle R \rangle}{6\Delta t} = \frac{\sum_{i=1}^{N}(d_{xi}^2 + d_{yi}^2 + d_{zi}^2)/N}{6\Delta t}, \tag{6}$$

where $\langle R \rangle$ is the mean square displacement of all particles, N is the particle number and d_{xi}, d_{yi}, d_{zi} are the $i-$th particle displacements in the directions x, y and z over the time period Δt. The studies that have developed methods for evaluating the diffusion coefficient of substances in the brain will be discussed in Section 2.4.2.

2.3. Reaction

While the diffusion term in drug delivery models represents the physical transport of drug particles in the ECS, the reaction term accounts for drug elimination due to biochemical interactions between drug molecules and cells. Enzyme kinetic models, a class of mathematical models that describe the rate of enzyme-catalyzed chemical reactions, can be used to describe the drug reaction process. One of the most widely adopted models is the Michaelis-Menten model, *i.e.*

$$V = \frac{V_{\max} C}{K_m + C}, \tag{7}$$

which describes the rate of enzymatic reactions by relating the reaction rate to the concentration of a substrate. In Eq. (7), V is the reaction rate, $V_{\max}$ is the maximum reaction rate, C is the substrate concentration and K_m is the Michaelis constant, which represents the substrate concentration at which the reaction rate is half of $V_{\max}$. Researchers have used the Michaelis-Menten kinetics model to describe the active transport of drugs into or out of the nerve cells [23,55–57].

By defining the reaction rate as a function of drug concentration, this model can be perfectly integrated into the convection-diffusion equation. However, this also represents a significant limitation of the model, as the rate of drug reaction is generally not determined by concentration alone. It is also worth mentioning that the Michaelis constant K_m varies depending on the type of drugs and cells and must be carefully calibrated. Therefore, more sophisticated kinetics models are required to describe drug reactions in the brain [58].

2.4. Supporting techniques

The supporting methods for the above-mentioned studies mainly include experimental and numerical characterization of hydraulic permeability, diffusion coefficient and reaction rate required to solve the established biomechanical models, as well as experimental observations of unknown phenomena to develop new biophysical laws.

2.4.1. Characterization of hydraulic permeability

The characterization of hydraulic permeability has been a long-standing research topic since the introduction of Darcy's law in 1856. Based on Darcy's law, the typical method is to apply a pressure gradient across the sample and measure the flow rate of the fluid flowing through the sample [59–61], as shown in Fig. 2A, and referred to as the perfusion method. Tavner et al. [62] used this method to measure the hydraulic conductivity of lamb and sheep brains.

Compression is also a commonly used method for indirectly measuring hydraulic permeability. Based on the consolidation theory, which considers the equilibrium between the hydraulic pressure inside the pores and the stress of the matrix caused by compression, the relationship between the flow rate due to pore deformation and the hydraulic pressure can be obtained to calcu-

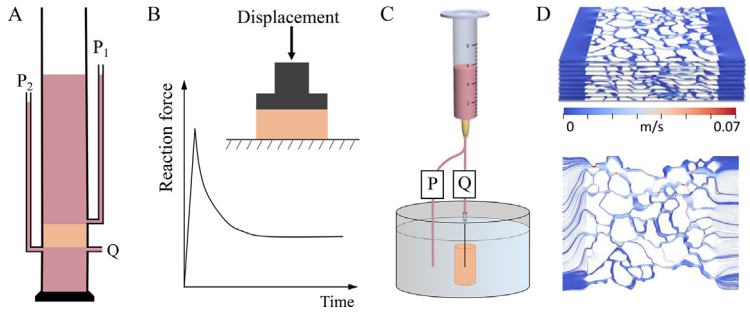

Fig. 2. Methods for characterizing the hydraulic permeability of brain tissue: (A) Perfusion method. Orange block represents the tissue, $P_1 - P_2$ stands for the pressure difference along the sample, and Q is the flow rate. (B) Unconfined compression method. (C) Infusion method, where P is the applied pressure difference and Q the flow rate. (D) Computational fluid dynamic method based on high-resolution imaging and reconstruction techniques; reproduced from Vidotto et al. [28].

late the permeability. There are two types of compression methods, namely unconfined compression and confined compression. In unconfined compression, as shown in Fig. 2B, fluid drains out of all boundaries of the sample. Using this method, Cheng and Bilston [63] and Su et al. [64] measured the permeability of calf brain and porcine brain, respectively. In confined compression, the fluid drains out from the top and bottom of the sample. Based on confined compression, Franceschini et al. [48] performed an uniaxial deformation experiment on human brain tissue within 12h after death and indirectly determined the permeability from the compressibility parameters by fitting the data to Terzaghi's theory.

However, for brain tissues, which are very soft, highly heterogeneous and less permeable, both the perfusion method and the compression method reach their limits. Low perfusion pressure gradients may not allow fluid to flow through the tissue, while high perfusion pressure gradients may compress the tissue and alter its microstructure, resulting in inaccurate values of measured permeability. This indicates that the parameters in the perfusion method should be determined very carefully. In addition, the compression method definitely deforms the microstructure. Under these circumstances, the infusion method, which involves injecting fluid into tissue while monitoring the flow rate and injection pressure, as shown in Fig. 2C, can be applied [65–67]. Furthermore, the infusion method offers the advantage of capturing local permeability, which cannot be explicitly measured using the perfusion and compression methods in nonuniform tissues. Using the infusion method, Jamal et al. [24] measured the localized anisotropic permeability tensor of the ovine brain WM under different infusion pressure. Importantly, this study found that the brain permeability is pressure dependent. Subsequent theoretical studies [13,23] revealed that this is caused by the interactions between the infused fluid and the axons. These studies demonstrated the significant effects of pressure-driven neuronal deformation on the permeability tensor of brain WM. Subsequently, a new pressure-dependent permeability tensor for brain WM was proposed, which complements the classical Darcy's law and can quantitatively consider the effects of infusion pressure on the drug-delivery process in the brain [13].

Numerical methods can also be employed to derive hydraulic permeability because pressure drop and flow rate can be calculated by solving the NS equations in the pore-scale geometry. For example, based on simplified geometries and realistic geometries at the neuron level, Vidotto et al. [22,28] characterized the permeability tensors of brain tissue in different regions using computational fluid dynamics (CFD) simulations. Their study showed high heterogeneity of hydraulic permeability in different regions of the brain, which to some extent explains the failure in drug delivery to the brain caused by CED, especially the observed uneven distribution of drug volume and concentration [7,8]. Motivated by the uncertainty of brain permeability due to microstructural heterogeneity, in a recent study Yuan et al. [49] proposed a mathematical expression that links the microstructural information of brain WM with its permeability tensor, using mathematical derivation, CFD modeling and stochastically reconstructed brain WM geometry obtained from high-resolution imaging (FIB-SEM) data. This study was able to fill this gap and provide more accurate predictions about the pathway of drug delivery in brain tissue. However, from an imaging perspective, further efforts are required to capture the microstructural information *in vivo*. Importantly, Su et al. [68] found that wettability significantly influences the permeability of brain WM and that the effects are anisotropic. This shows the importance of adjusting the boundary conditions when using CFD to characterize the permeability of brain WM.

2.4.2. Characterization of the diffusion coefficient

Characterizing the diffusion coefficient of molecules or particles in the brain is a challenging task. According to Section 2.2, either the concentration gradient (macroscale, Fick's Law Eq. (5)) or the motions of individual particles (microscale, Einstein's diffusion equation Eq. (6)) must be known to be able to calculate the diffusion coefficient.

Based on Fick's law, Nicholson and Tao [69] developed a concentration-based method called integrative optical imaging (IOI) technique to measure the diffusion coefficient of fluorescent dextran molecules in the agarose gel and in the extracellular microenvironment of the brain. As demonstrated in Fig. 3A, they injected a known amount of fluorescent molecules (*i.e.*, a known concentration) into the tissue and then took images of the fluorescence over time using a microscope. By analyzing the changes in fluorescence intensity in the images, they were able to calculate the apparent diffusion coefficient (ADC) of the dextran molecules. In addition, by analyzing the diffusion of particles of different sizes, Thorne and Nicholson [70] found that the extracellular space (ECS) of brain tissue has a normal width of 38 to 64 nm, which has a great impact on subsequent studies related to the brain micro-environment, *e.g.*, drug development and delivery [71–73], metabolic waste clearance [37,74], and treatments of brain cancer [73,75]. Similarly, Valnes et al. [76] developed a mathematical contrast approach to measure the diffusion coefficient of the CSF tracer in the cortical GM of the human cerebral cortex. The authors used the diffusion equation to model the concentration of a tracer injected into the CSF of the brain. By comparing the results of their model with the observed CSF tracer concentrations from magnetic resonance imaging (MRI) scans, they were able to estimate the ADC that best fit the data.

Einstein's diffusion equation provides the fundamental theory for the numerical characterization of the diffusion tensor, since the trajectory of the particles can be solved based on Newton's second law once the forces acting on the particles are described mathematically. For example, Su et al. [26] developed a particle trajectory tracking model that can account for particle dynamics in

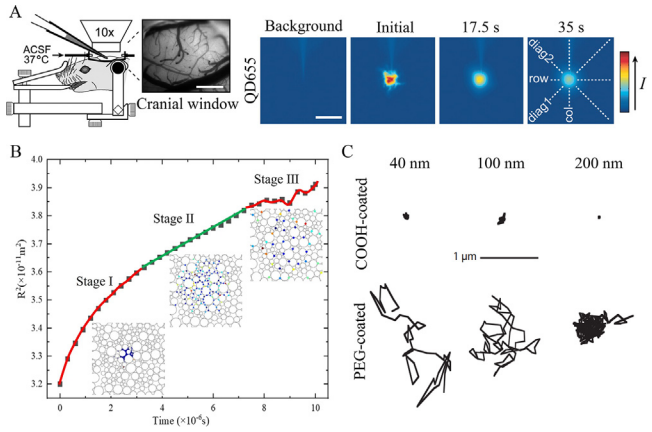

Fig. 3. Diffusion in the brain: (A) *In vivo* measurement of particle diffusion in the brain. Consecutive images of fluorescent intensity *I* were taken with a cooled charge-coupled device camera through a microscope with a ×10 water-immersion objective after pressure ejection from a micropipette into the rat brain accessible through an open cranial window (scale bar: 500 μm); reproduced from Thorne and Nicholson [70]. (B) Typical mean square displacement relationship over time of nanoparticles in brain WM; reproduced from Yuan et al. [27]. (C) Representative particle trajectories for COOH- and PEG-coated nanoparticles of various sizes in human brain tissue at a time scale of 1 s; reproduced from Nance et al. [71].

an aqueous solution and the interactions of the particles with a spherical surface, which allowed the authors to calculate the diffusion tensor of particles. However, in this study, the microstructure of the porous medium was not considered, which means that the model may not be valid if the particle size is not negligible compared to the pore size. A new framework developed by Yuan et al. [27] that embeds a particle tracking model into the neuron-scale microstructure of the brain WM narrows the gap and is able to estimate the diffusion coefficient of nanoparticles (NPs) up to the ECS width of the brain WM. The authors obtained the typical relationship between the mean squared displacement and the time of charged NPs in the brain WM, as shown in Fig. 3B. The slope of the Stage II curve is the diffusion coefficient. The accuracy obviously depends on the accuracy of the reconstructed microstructure. The Brownian force due to molecular thermal motion, the drag force of the fluid environment, and the electrical forces due to the charge properties of particles and neurons are the most commonly considered forces in the reported models. Further investigation demonstrated the ability of this model to explore new drug delivery techniques, such as achieving isotropic drug distribution in anisotropic brain tissue by applying magnetic NPs and an external magnetic field [77]. Nance et al. [71] has also successfully measured the ADC of particles with different surface coatings in the brain parenchyma by adopting the multiple particle tracking method to record particle trajectories, as shown in Fig. 3C. The advanced particle tracking methods also allow researchers to explicitly observe the particle-brain interactions in the brain micro-environment. These provide strong evidence for developing a deeper understanding of particle behavior in the brain and for creating more precise models, *e.g.*, models based on molecular dynamics (MD) simulations [78,79] to characterize the reaction term of the transport processes. The recent advances and capabilities of particle tracking methods have been discussed in detail in [80,81].

2.4.3. Characterization of the reaction rate

From a macroscale perspective, clearance is the most important measure of drug reaction. It can be defined as the theoretical volume of fluid from which a drug is completely removed per unit time [82]. In other words, clearance represents the rate at which the drug is removed from the body. The clearance rates of some commonly used brain tumor drugs can be found in [29].

To explicitly account for individual drug molecules, the reaction rate of drugs can also be assessed through MD modeling. Compared with the particle trajectory tracking model discussed in the above section, MD has inherent advantages in terms of accuracy because the objects of MD are atoms and molecules that form the drug particles and cell surfaces. Therefore, far fewer hypotheses are needed in the simulations, aside from the availability of accurate potentials to describe atomic and molecular interactions, which is essential to avoid deviation or the inability to capture the fundamental interactions of interest. Consequently, MD has been widely used to model particle-cell interactions. Shi and co-authors have performed extensive experimental and MD studies to investigate the process of molecules and NPs entering into cells. For example, they used the method of coarse-grained molecular dynamics to theoretically analyze the entry process of one-dimensional nanomaterials into the cell [78]. The results showed that the caps or shells at the tip of NPs have a significant effect on the nature of membrane interaction. Further studies were conducted to investigate the influence of other factors on the molecular-membrane interactions, including size [83–85], shape [78,86], and chemical and physical properties of the molecules [87,88].

2.4.4. Imaging techniques for microstructure reconstruction

Numerical characterization of the hydraulic permeability and diffusion coefficient as mentioned in Sections 2.4.1 (represented by Fig. 2D) and 2.4.2 (represented by Fig. 3B) are gaining increasing attention as high-resolution imaging techniques become more accessible for neuron-scale microstructural reconstruction [27,28,89]. Rapid advances in these techniques over the past two decades have led to noticeable improvements in both higher resolution and the ability to segment and reconstruct brain microstructure with increased accuracy and varying degrees of automation [90,91]. The most commonly used techniques include:

(i) Scanning electron microscopy (SEM): a type of electron microscope that creates images of a sample by scanning its surface with a focused beam of electrons. The electrons interact with atoms in the sample and produce various signals that contain information about the surface topography and composition of the sample.
(ii) Transmission electron microscopy (TEM): a microscopy technique in which a beam of electrons is transmitted through an ultra-thin specimen (usually less than 100 nm) to produce an image. The electrons interact with the sample as the beam passes through it, and an image is formed from this interaction. Due to the smaller de Broglie wavelength of electrons, TEMs are image with a significant higher resolution than light microscopes. This allows the instrument to capture fine details, even as small as a single column of atoms.
(iii) Focused ion beam-scanning electron microscopy (FIB-SEM): a technique that combines a focused ion beam (FIB) and a scanning electron microscope (SEM) on the same platform. The FIB can be used to remove or deposit materials on the sample surface, while the SEM can be used to image the surface with electrons. FIB-SEM can create two-dimensional (2D) and three-dimensional (3D) images of surface topography and resolve nm-scale features. FIB-SEM can also integrate diffraction and X-ray spectroscopy for microstructural analysis.
(iv) Micro-computed tomography (μ-CT): a non-destructive imaging tool that produces high-resolution 3D images consisting of 2D trans-axial projections or 'slices' of a target specimen. μ-CT is similar to hospital CT imaging, but on a smaller scale and with significantly higher resolution. It allows examining the internal structure of an object without having to destroy it.

Theoretically, they all have the ability to microstructurally reconstruct brain tissue, but they have their specific advantages and

disadvantages. For example, while SEM and TEM have higher resolution compared to μ-CT, they are destructive. FIB-SEM is capable of producing high-resolution 3D images, but is time-consuming. A systematic comparison between these techniques, including other 3D imaging modalities, *e.g.*, confocal optical microscopy, neutron tomography and MRI, was carried out by Vásárhelyi et al. [92].

3. Solid mechanics: brain tissue properties and needle-tissue interaction

As an invasive drug delivery method to physically bypass the BBB, CED operations will inevitably lead to brain deformation and damage [93]. The deformation may further change the local microstructure and pathways for drug transport, thus affecting the efficiency of drug delivery [13,29]. In addition, the brain-needle interaction can alter the penetration path of the needle, especially when using flexible catheters designed for robotic needle steering, which can also affect drug delivery efficacy [94,95]. The principles of solid mechanics are therefore essential to understand, predict and minimize tissue damage caused by invasive drug delivery to the brain.

3.1. Properties and constitutive models of brain tissues

3.1.1. Nonlinearity

Based on experimental and theoretical methods, it is widely accepted that brain tissue deforms similarly to soft porous elastomers, with an intricate response governed by large deformations, pre-conditioning, and rate-dependent behavior at different time scales [33,96]. Various strain-energy functions for brain tissue have been proposed in the literature, including Mooney-Rivlin [97,98], Fung [97], Gent [97], Ogden [97–102] and some polynomial formulations [100,103–105]. In addition, the mechanical properties of brain tissue are heterogeneous, region- and age-dependent [106–112]. GM usually appears stiffer than WM in large-strain compression, tension and shear experiments [110], while the opposite trend is observed for indentation [109,112–116].

3.1.2. Rate-dependence

Rate-dependence in brain tissue is traditionally related to viscoelasticity and has been modeled using various approaches based on linear or quasi-linear viscoelasticity [97–105,108,115,117,118], fractional viscoelasticity [119,120], and nonlinear viscoelastic models [121–124]. Given the extreme softness of brain tissue, several studies have emphasized the importance of considering nonlinear deformations in brain tissue mechanics. Nonlinear viscoelasticity is usually based on a kinematic multiplicative split of the deformation gradient tensor $\mathbf{F}$ into an elastic part (labeled by the subscript e) and a viscous part (labeled by the subscript v), so that $\mathbf{F}=\mathbf{F}_\mathrm{e}\mathbf{F}_\mathrm{v}$. As a result, one can obtain a decoupled representation of the strain-energy function and of the Cauchy stress tensor [125], namely

$$\Psi(\mathbf{C})=\Psi^{\mathrm{eq}}(\mathbf{C})+\Psi^{\mathrm{neq}}(\mathbf{C}_\mathrm{e}), \tag{8a}$$

$$\boldsymbol{\sigma}=\boldsymbol{\sigma}^{\mathrm{eq}}+\boldsymbol{\sigma}^{\mathrm{neq}}=2J^{-1}\mathbf{F}\frac{\partial\Psi^{\mathrm{eq}}}{\partial\mathbf{C}}\mathbf{F}^{\mathrm{T}}+2J^{-1}\mathbf{F}_\mathrm{e}\frac{\partial\Psi^{\mathrm{neq}}}{\partial\mathbf{C}_\mathrm{e}}\mathbf{F}_\mathrm{e}^{\mathrm{T}}, \tag{8b}$$

where $\mathbf{C}=\mathbf{F}^{\mathrm{T}}\mathbf{F}$ is the right Cauchy–Green tensor, $\mathbf{C}_\mathrm{e}=\mathbf{F}_\mathrm{e}^{\mathrm{T}}\mathbf{F}_\mathrm{e}$ is the elastic part and $J=\det\mathbf{F}>0$ is the volume ratio. It may be beneficial to visualize this decomposition with a classical rheological model, borrowed from linear viscoelasticity, in which the strain-energy function Ψ^{eq} and the associated stress $\boldsymbol{\sigma}^{\mathrm{eq}}$ represent the contribution of an elastic spring, while Ψ^{neq} is the strain energy in the spring-dashpot element and $\boldsymbol{\sigma}^{\mathrm{neq}}$ the associated stress. Note that there is no restriction on the specific form of the strain-energy functions that enter into Eq. (8).

It is worth mentioning that some studies claim that the applicability of linear models should not be ruled out. At low loading rates, which is usually the case in drug delivery and device implantation, linear viscoelasticity might provide reliable results and ensure higher efficiency [98,108,112].

3.1.3. Anisotropy

Some experimental studies suggest that WM regions of the brain exhibit mechanical anisotropy, probably due to the bundles of axonal fibers that can be highly aligned along a preferential direction, such as in the corpus callosum [98,106,107,126,127]. Therefore, WM models based on those developed for fiber-reinforced soft tissues have been proposed [11,126,128–130]. However, the anisotropic nature of brain tissue is still controversial, and other studies assumed that the mechanical anisotropy is marginal [102,110,131] and the structural anisotropy of the tissue is only relevant to the diffusion or permeability properties [24,29]. Part of the discrepancy may depend on the different scale and loads at which the tissue samples were tested [132]. Here, we assume that the strain-energy terms appearing in Eq. (8) are isotropic functions, leaving open the possibility of extending this framework to anisotropy, but at the expense of a more cumbersome numerical treatment [133]. Assuming isotropy, the strain-energy function and the associated Cauchy stress tensor of the viscoelastic brain tissue are expressed as [123]

$$\Psi(\mathbf{b})=\Psi^{\mathrm{eq}}(\mathbf{b})+\Psi^{\mathrm{neq}}(\mathbf{b}_\mathrm{e}), \tag{9a}$$

$$\boldsymbol{\sigma}=\boldsymbol{\sigma}^{\mathrm{eq}}+\boldsymbol{\sigma}^{\mathrm{neq}}=J^{-1}\sum_{a=1}^{3}\lambda_a\frac{\partial\Psi^{\mathrm{eq}}}{\partial\lambda_a}\mathbf{n}_a\otimes\mathbf{n}_a +J^{-1}\sum_{a=1}^{3}\lambda_{a,\mathrm{e}}\frac{\partial\Psi^{\mathrm{neq}}}{\partial\lambda_{a,\mathrm{e}}}\mathbf{n}_{a,\mathrm{e}}\otimes\mathbf{n}_{a,\mathrm{e}}, \tag{9b}$$

where λ_a, $a\in 1,2,3$, are principal stretches representing the eigenvalues of the left Cauchy–Green tensor $\mathbf{b}=\mathbf{F}\mathbf{F}^{\mathrm{T}}=\sum_{a=1}^{3}\lambda_a^2\,\mathbf{n}_a\otimes\mathbf{n}_a$, where $\mathbf{n}_a$ are the principal directions of the material in the current configuration. The elastic principal stretches $\lambda_{a,\mathrm{e}}$ and principal directions $\mathbf{n}_{a,\mathrm{e}}$ are defined analogously from the elastic left Cauchy–Green tensor $\mathbf{b}_\mathrm{e}=\mathbf{F}_\mathrm{e}\mathbf{F}_\mathrm{e}^{\mathrm{T}}$. This tensor represents the viscoelastic history variable and is obtained from the solution of an appropriate rate equation (generally one for each spring-dashpot element introduced to approximate the relaxation of the material), which needs to ensure a non-negative viscous dissipation $\mathcal{D}_\mathrm{v}$. For example, Budday et al. [123] adopted the following rate equation [125]: $-\mathcal{L}_{\boldsymbol{v}}\mathbf{b}_\mathrm{e}\mathbf{b}_\mathrm{e}^{-1}=(J/\eta)\boldsymbol{\sigma}^{\mathrm{neq}}$, where η is the viscosity of the solid and $\mathcal{L}_{\boldsymbol{v}}$ denotes the Lie derivative [134]. The viscous dissipation rate is then calculated as $\mathcal{D}_\mathrm{v}=(J^2/2\eta)\boldsymbol{\sigma}^{\mathrm{neq}}:\boldsymbol{\sigma}^{\mathrm{neq}}$ [135].

3.1.4. Compressibility

Another fundamental aspect of brain tissue mechanics is related to volumetric deformations. It is generally accepted that viscous relaxation has no influence on the volumetric response [121,123], so that the non-equilibrium term in Eq. (9) becomes purely deviatoric. In addition, similar to elastomers, the volumetric component is usually decoupled from the total deformation, so the equilibrium Cauchy stress is given as $\boldsymbol{\sigma}^{\mathrm{eq}}=\boldsymbol{\sigma}^{\mathrm{eq}}_{\mathrm{iso}}+\boldsymbol{\sigma}_{\mathrm{vol}}$, where $\boldsymbol{\sigma}^{\mathrm{eq}}_{\mathrm{iso}}$ is the deviatoric equilibrium stress and $\boldsymbol{\sigma}_{\mathrm{vol}}$ is the term associated to the volumetric deformations. In several studies, brain tissue is assumed to be incompressible, meaning that the volumetric term $\boldsymbol{\sigma}_{\mathrm{vol}}=-p\mathbf{I}$ is a means to enforce incompressibility through a Lagrange parameter p [121,123]. However, as discussed later in this section, brain tissue is highly hydrated and the motion of the interstitial fluid must be reflected in the bulk response of the material. For example, Prevost et al. [122] proposed the following expression for the

volumetric stress, *i.e.*

$$\boldsymbol{\sigma}_{\text{vol}} = K \ln\left(\frac{J - f_1}{1 - f_1}\right)\mathbf{I}, \tag{10}$$

where K is the bulk modulus and $\mathbf{I}$ denotes the second-order identity tensor. The scalar f_1 represents the incompressible volume fraction of the material and defines the so-called compaction point of the material, that is, the volumetric stress becomes infinite for $J \to f_1$ [122].

3.1.5. Biphasic and poro-elastic properties

The effects of fluid-solid interaction (FSI) between fluids and cells are a fundamental part of the mechanical behavior of brain tissue and are involved in the healthy and pathological physiology of the human brain [136–138]. Although it is quite common in the brain tissue literature to include rate-dependent behavior only in the framework of viscoelasticity [62,103], the interaction between brain tissue deformation and fluid transport is crucial in the context of drug delivery. Modeling approaches that consider the presence of a fluid phase in the brain are based on the theory of porous media, which approximates the brain tissue as a biphasic material. The basic biphasic theory assumes that the tissue is a mixture of an elastic solid phase and an inviscid fluid phase. The relative motion between these two phases results into a form of dissipation that determines the characteristic relaxation in the soft tissue. This approach, formalized by Bowen [139] and first applied to biological tissues for articular cartilage by Mow et al. [140], was also adapted to the brain [141]. More recently, it has been combined with viscoelasticity to describe flow-independent dissipation [135,142–144] and with a growth term to account for tumor proliferation [145]. In parallel, another modeling approach was derived from Biot's classical consolidation theory [146,147], and applied to the brain within the infinitesimal strain theory [48,148–151] or nonlinear poroelasticity [101,152–155].

Specifically, the brain tissue is modeled as a biphasic medium consisting of a solid phase, including the network of cells and capillaries embedded in the ECS, and a fluid phase consisting of interstitial fluid surrounding the neurons [135]. These two phases are characterized by mass densities $\rho_{\text{F}}, \rho_{\text{S}}$ and volume fractions $n_{\text{F}}, n_{\text{S}}$, which we assume to satisfy the condition of saturation $n_{\text{F}} + n_{\text{S}} = 1$. The theory is developed within the framework of nonlinear kinematics and requires the fundamental mass and momentum balances for the biphasic medium [156]. In the current configuration these are expressed as

$$\nabla \cdot (n_{\text{F}}\mathbf{w}_{\text{F}}) + \dot{\overline{\ln J}} = 0, \tag{11a}$$

$$\nabla \cdot (\boldsymbol{\sigma}_{\text{F}} + \boldsymbol{\sigma}_{\text{S}}) + \rho\mathbf{f} = \mathbf{0}\,. \tag{11b}$$

The mass balance in Eq. (11a) equates the rate of volume change of the biphasic medium with the outflow of fluid and is derived assuming the incompressibility of the single phases. Here $\mathbf{w}_{\text{F}}$ is the seepage velocity, a relative velocity of the fluid with respect to the deforming solid, and J is the volume ratio, which describes the volume change in the biphasic medium. In the balance of linear momentum for quasi-static conditions, written in Eq. (11b), $\mathbf{f}$ is the vector of body forces per unit volume and $\rho = n_{\text{F}}\rho_{\text{F}} + (1 - n_{\text{F}})\rho_{\text{S}}$ is the homogenized density. This expression for the biphasic medium is derived by considering the Cauchy stress tensor in the single phases and the interaction terms, which we express as

$$\boldsymbol{\sigma}_{\text{F}} = -n_{\text{F}}p\mathbf{I}, \qquad \boldsymbol{\sigma}_{\text{S}} = \boldsymbol{\sigma}_{\text{S}}^{\text{E}} - n_{\text{S}}p\mathbf{I}, \tag{12a}$$

$$\tilde{\boldsymbol{p}}_{\text{F}} = -\tilde{\boldsymbol{p}}_{\text{S}} = p\nabla n_{\text{F}} + \tilde{\boldsymbol{p}}_{\text{F}}^{\text{E}}\,. \tag{12b}$$

Eq. (12a) defines the *extra* stress in the solid matrix $\boldsymbol{\sigma}_{\text{S}}^{\text{E}}$, similar to the concept of effective stress in Biot's classical consolidation theory and assumes that the shear stresses of the fluid are negligible. The internal friction exerted between the solid and the fluid is modeled by the exchange term $\tilde{\boldsymbol{p}}_{\text{F}}^{\text{E}}$ in Eq. (12b), which therefore provides the fluid-dependent dissipative contribution in the model.

The theory is completed by suitable constitutive models for the solid and fluid phases. The constitutive behavior of the fluid in the biphasic medium is governed by the generalized Darcy's law, which was introduced in Eq. (4), where $\mathbf{w} = n_{\text{F}}\mathbf{w}_{\text{F}}$. With this assumption, the fluid-dependent dissipation rate can be calculated from the interaction term as $\mathcal{D}_{\text{f}} = -\tilde{\boldsymbol{p}}_{\text{F}}^{\text{E}} \cdot \mathbf{w}_{\text{F}} = \mu_{\text{F}}\boldsymbol{\kappa}^{-1}\mathbf{w} \cdot \mathbf{w}$ [135].

Note that the hydraulic permeability tensor $\boldsymbol{\kappa}$ appearing in Darcy's law (4) is a spatial tensor that is generally anisotropic [157]. Ehlers and Eipper [156] proposed a power law form to account for the dependence of the hydraulic permeability on deformation, *i.e.*

$$\boldsymbol{\kappa} = \left(\frac{J - n_{0,\text{S}}}{1 - n_{0,\text{S}}}\right)^m \boldsymbol{\kappa}_0, \tag{13}$$

where $\boldsymbol{\kappa}_0 = \kappa_0\mathbf{I}$ is an isotropic material tensor, $m \geq 0$ is a parameter, $n_{0,\text{S}}$ is the initial solid volume fraction and κ_0 is the *intrinsic* hydraulic permeability, a material property. Due to the microstructural complexity of brain tissues, the porosity of the tissue (ϕ or n_{F} in mixture theory) cannot uniquely determine its permeability tensor [49]. Yuan et al. [13] has developed a permeability tensor as a function of local pressure and pressure gradient, providing an accurate alternative to consider the deformation-dependent permeability of brain tissue. This function was derived by explicitly modeling the dynamic interactions between axonal deformation and fluid flow, as shown in Fig. 4.

The constitutive model for the solid phase may include nonlinear elastic or viscoelastic terms. Although the individual phases are incompressible, it is required to include a term that allows for large volume changes that can occur as a result of changes in volume fractions [156]. Following the framework introduced by Eq. (9), Comellas et al. [135] proposed two Ogden strain-energy functions for the equilibrium and non-equilibrium parts of the solid, so that the Cauchy extra stress in the solid matrix is expressed as

$$\boldsymbol{\sigma}_{\text{S}}^{\text{E}} = \boldsymbol{\sigma}_{\text{S,iso}}^{\text{eq}} + \boldsymbol{\sigma}_{\text{vol}} + \boldsymbol{\sigma}_{\text{S,iso}}^{\text{neq}}, \tag{14a}$$

$$\boldsymbol{\sigma}_{\text{S,iso}}^{\text{eq}} = J^{-1}\mu_\infty \sum_{a=1}^{3}\left[\bar{\lambda}_a{}^{\alpha_\infty} - \frac{1}{3}\left(\bar{\lambda}_1{}^{\alpha_\infty} + \bar{\lambda}_2{}^{\alpha_\infty} + \bar{\lambda}_3{}^{\alpha_\infty}\right)\right]\mathbf{n}_a \otimes \mathbf{n}_a, \tag{14b}$$

$$\boldsymbol{\sigma}_{\text{S,iso}}^{\text{neq}} = J^{-1}\mu \sum_{a=1}^{3}\left[\bar{\lambda}_{a,\text{e}}{}^{\alpha} - \frac{1}{3}\left(\bar{\lambda}_{1,\text{e}}{}^{\alpha} + \bar{\lambda}_{2,\text{e}}{}^{\alpha} + \bar{\lambda}_{3,\text{e}}{}^{\alpha}\right)\right]\mathbf{n}_{a,\text{e}} \otimes \mathbf{n}_{a,\text{e}}, \tag{14c}$$

where we have introduced the Ogden moduli and nonlinear parameters $\mu_\infty, \alpha_\infty$ and μ, α in the equilibrium term $\Psi_{\text{S}}^{\text{eq}}$ and the non-equilibrium term $\Psi_{\text{S}}^{\text{neq}}$, respectively. In Eq. (14b), $\bar{\lambda}_a$ are isochoric principal stretches that represent the eigenvalues of the isochoric left Cauchy–Green tensor and $\bar{\mathbf{b}} = J^{-2/3}\mathbf{F}\mathbf{F}^{\text{T}} = \sum_{a=1}^{3}\bar{\lambda}_a^2\,\mathbf{n}_a \otimes \mathbf{n}_a$, and analogously for their elastic counterparts in Eq. (14c). The volumetric Cauchy stress tensor in Eq. (14a) is given by Comellas et al. [135]

$$\boldsymbol{\sigma}_{\text{vol}} = \Lambda(1 - n_{0,\text{S}})^2\left(\frac{1}{1 - n_{0,\text{S}}} - \frac{1}{J - n_{0,\text{S}}}\right)\mathbf{I}, \tag{15}$$

where Λ is the second Lamé parameter related to the bulk modulus. Eq. (15) is similar to Eq. (10), but here the evolution of the

Table 2
Mechanical properties of brain tissue obtained using different methods (GM = gray matter; WM = white matter).

Tissue types and region	Material model	Loading condition	Refs.
Swine brain	Hyper-viscoelastic model	indentation, *in vivo**	[158]
Swine brain	Hyper-viscoelastic model	tension and unconfined compression (strain in $< -0.3, 0.2 >$)	[99]
Porcine brain GM and WM	Modified Ogden hyperelastic model	shear and compression	[106]
Porcine brain cerebral cortex	Hyper-viscoelastic model	indentation, *in vivo, in situ*, and *in vitro*	[159]
Human brain GM and WM	Poro-viscoelastic model	cyclic loading, failure, confined compression	[48]
Calf brain WM	Poro-viscoelastic model	unconfined compression	[142]
Bovine brain GM and WM	Linear elastic model	tension	[160]
Bovine brain GM and WM	Anisotropy rate-dependent model	high strain-rate compression (up to 3000/s)	[131]
Porcine brain mixed GM and WM samples	Large strain, nonlinear, viscoelastic model	cyclic unconfined compression	[122,161]
Porcine brain GM and WM	Elastic and Yeoh hyperelastic models	indentation, *in vitro*	[162]
Porcine brain multiple regions	Quasi-linear viscoelastic	multistep indentation	[108]
Bovine brain	Quasi-linear viscoelastic model hyperelastic material	finite step-and-hold uniaxial unconfined compression	[104]
Porcine brain mixed GM and WM samples	One-term Ogden model	unconfined compression strain rates ≤ 90/s	[163,164]
Lamb brain WM	Transversely isotropic hyperelastic model	indentation	[126]
Porcine brain mixed GM and WM samples	Ogden and Mooney-Rivlin models	simple shear test at strain rates ≤ 120/s	[97]
Human brain multiple regions	Isotropic modified one-term Ogden model	simple shear in two orthogonal directions, unconfined compression, and tension	[110]
Brain	Visco-hyperelastic model	tension/unconfined compression	[165]
Porcine brain multiple regions	Linear viscoelastic model	multistep stress relaxation indentations	[98]
Bovine brain different WM regions	Hyperelastic, strain-stiffening in compression and strain-softening in tension	uniaxial tension and unconfined compression	[166]
Sheep brain, WM regions	Two-term prony series	microindentation	[127]
Human brain, fresh, post-operative, GM and WM	Linear viscoelastic	multistep indentation	[112]
Göttingen minipigs brain multiple regions	Unidirectional hyper-viscoelastic models with an Ogden hyperelastic representation and a single-term Prony series, strain rate stiffening in both shear and compression	simple shear and unconfined compression	[167]

**In vivo* experiments are listed; no information means *in vitro* experiments.

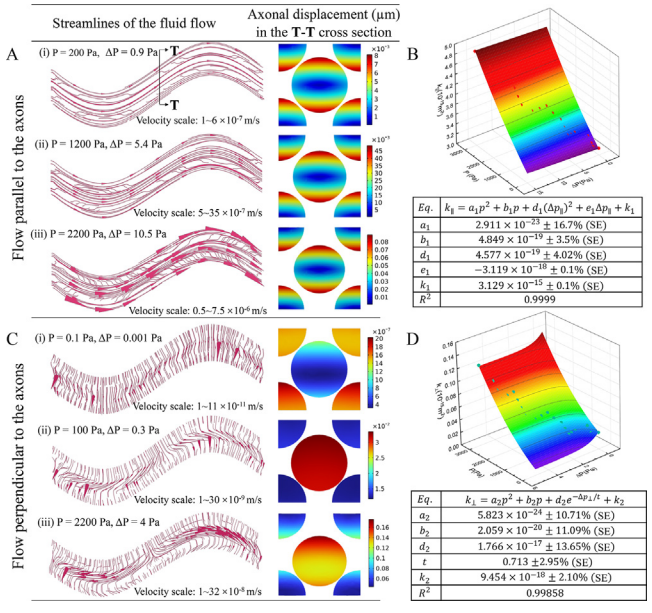

Fig. 4. Derivation of the brain white matter permeability tensor as a function of pressure and pressure drop by explicitly modeling the fluid-solid interaction between the interstitial fluid and the axons; reproduced from Yuan et al. [13]: (A) Parallel flow status and axonal displacement. The streamlines on the left side of the figures indicate the flow direction. The cone size of the streamlines is proportional to the flow velocity magnitude and the scaling factors are indicated below the streamlines. The images on the right show the axonal displacement in the central cross section (*i.e.* the **T-T** cross section as annotated in the streamline image). (B) Permeability in the parallel direction as a function of pressure and pressure drop (*i.e.* $\kappa_{\parallel} = f(p, \Delta p)$) derived by surface fitting. The tables show the fitting equations, values of the coefficients ± standard error (SE) as a percentage of the coefficients, and the R^2 of each fitting result. (C) Perpendicular flow status and axonal deformation. (D) Permeability in the perpendicular direction as a function of pressure and pressure drop (*i.e.* $\kappa_{\perp} = f(p, \Delta p)$).

volume fraction depends on the continuity equation of the biphasic medium.

Table 2 summarizes the mechanical properties of brain tissue in terms of tissue types, tissue regions, constitutive model and loading conditions obtained by experimental tests. The adoption of a specific material model depends on the application. In the condition of hydrocephalus, which resembles the drug transport process in the brain, Gholampour et al. [137,138] suggested that the most optimal material properties for the brain are 'poro-visco-elastic'. This can be an important reference when selecting material models for modeling drug delivery in the brain.

3.2. Needle-tissue interaction during infusion-based drug delivery

The deformation of brain tissue caused by infusion-based drug delivery occurs in several stages [168,169]. As illustrated in Fig. 5, it includes tissue compression, contact with friction, and rupture. In general, both the tangential stress $\mathbf{t}_s$ and the normal stress $\mathbf{t}_n$ provide an energetic contribution entering Eq. 16 and directly affect the tissue rupture[170,171]. Subsequently one can observe local tissue swelling due to drug injection [172], tissue-needle separation due to backflow [173], and recovery of tissue viscosity with drug absorption and outflow from the injection site. If the pressure is too high, local tissue damage can occur. Capturing these phenomena requires a combination of theoretical principles and targeted experiments.

Studies of needle-tissue interaction in the brain began about 20 years ago. However, despite the relevance of such phenomena, there are few studies directly targeting the brain, which may be partly due to limited access to brain samples and data. Fortunately, there are a number of related studies on various soft tissues or tissue phantoms that could provide useful insights for needle-brain studies.

The first attempt to model the needle-tissue interaction resulted in low-resolution numerical models based on phenomeno-

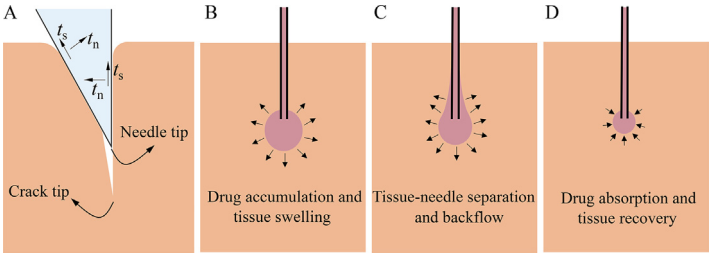

Fig. 5. Types of tissue deformation during the needle insertion process: (A) Tissue rupture and shear deformation; $\mathbf{t}_n$ stands for normal stress and $\mathbf{t}_s$ for shear stress due to friction. (B) Local tissue swelling due to drug accumulation. (C) Tissue-needle separation due to development of backflow. (D) Tissue recovery due to drug absorption and drainage.

logical expressions of the forces exerted by the needle on the substrate [174–177]. It is noteworthy that in these studies the tissue mechanics was based on the linearized theory of elasticity. In 2008, Wittek et al. [178] developed a continuum mechanics-based needle insertion model for the brain using a nonlinear viscoelastic constitutive model and patient-specific brain geometry reconstructed from MRI images. While this study assumed that brain tissue represented a single-phase continuum, other models for brain drug delivery developed the same period began to suggest the use of biphasic models [179,180]. However, the fundamental aspects of tissue rupture and needle-tissue interaction during penetration have been neglected, despite the proven importance of these factors [173].

The role of fracture mechanics in needle insertion has been investigated in several theoretical and numerical studies [181–183]. Accordingly, a versatile description of the needle insertion process provides an energy balance taking into account only mechanical work and quasi-static conditions. That reads [184]

$$\dot{W}_{\text{ext}} = \dot{W}_{\text{int}} + \dot{U}_{\text{f}} + \dot{\Gamma}\,. \tag{16}$$

The left-hand side of Eq. (16) represents the rate of change of the external mechanical work, W_{ext}, while the right-hand side stands for the rate of change of the internal energy of the system, W_{int}, the energy per unit time dissipated due to friction, U_{f} (equivalent to the effect of shear stress $\boldsymbol{t}_s$ in Fig. 5A), and the energy per unit time spent increasing the crack surface, Γ. The internal energy might also be responsible for the deformation of flexible needles commonly used in drug delivery and consists of a stored part $W^{\text{s}}_{\text{int}}$ and a dissipated part $W^{\text{d}}_{\text{int}}$ in a material with rate-dependent behavior. For example, with respect to the nonlinear biphasic viscoelastic model presented in Section 3.1, the internal energy is (with a rigid needle)

$$W^{\text{s}}_{\text{int}} = \int_v \left(\Psi^{\text{eq}}_{\text{S}} + \Psi^{\text{neq}}_{\text{S}}\right)\mathrm{d}v, \quad W^{\text{d}}_{\text{int}} = \int_v \int_t (\mathcal{D}_{\text{v}} + \mathcal{D}_{\text{f}})\mathrm{d}t\,\mathrm{d}v\,. \tag{17}$$

Now we introduce the assumption that the crack propagation occurs in a steady-state fashion, which implies that the rate of new crack surface formation is equivalent to the penetration rate of the needle [185]. Furthermore, the infinitesimal increment in time is proportional to the infinitesimal increment in the area A of the crack surface, which can be mathematically translated into $\partial/\partial t = \dot{A}\,\partial/\partial A$. Eq. (16) can then be re-written as

$$\frac{\partial}{\partial A}\left(W_{\text{ext}} - W^{\text{s}}_{\text{int}}\right) = G_0 + G_{\text{d}} + \frac{\partial}{\partial A}\left(W^{\text{d}}_{\text{int}} + U_{\text{f}}\right), \tag{18}$$

where G_0 is the intrinsic fracture energy of the material, and G_{d} is a rate-dependent contribution. Note that Eq. (18) for a purely elastic material and mode-I crack propagation, reduces to [182]

$$F\mathrm{d}u = \mathrm{d}W^{\text{s}}_{\text{int}} + F_{\text{f}}\mathrm{d}u + G_0 b\mathrm{d}u, \tag{19}$$

where $\mathrm{d}u$ is the increment of the needle displacement, b is the thickness of the material and F_{f} denotes the frictional force.

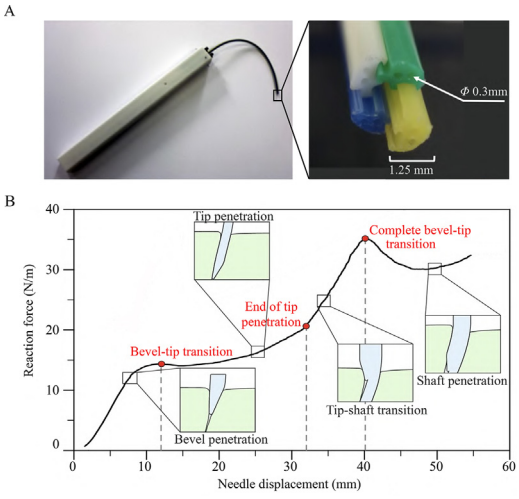

Fig. 6. Flexible needle for brain drug delivery and finite element modeling: (A) Programmable bevel-tip needle (PBN) for infusion-based brain drug delivery developed by Secoli et al. [95]. *Left*: Trocar with embedded medical grade PBN. *Right*: Cross section of the 4-segment PBN with two working channels with a diameter of 0.3 mm per segment. The overall diameter of the PBN is 2.5 mm. The figure is adapted from Secoli et al. [95]. (B) Typical force-displacement relationship obtained from the PBN insertion simulation. The simulation is based on an adaptive finite element algorithm developed by Terzano et al. [25]. The figure is adapted from Terzano et al. [25].

Advances in computational methods have enabled the incorporation of tissue rupture in large-scale finite element simulations of needle-tissue interaction [186] using cohesive zone models [25,94,187–190] or meshless methods [191]. Considering the new generation of steerable needles [95], Terzano et al. [25] have developed an adaptive finite element algorithm to handle the challenge that there is no predetermined penetration path, as shown in Fig. 6. This study showed that needle tip trajectories are highly dependent on the relative stiffness of the needle and tissue. In this study, a soft elastic phantom material was considered.

Regarding the effects of needle insertion in the tissue, Mahvash and Dupont [188] found that increasing insertion velocity leads to lower tissue rupture force and suggested applying a velocity inversely proportional to the relaxation time of the tissue to reduce tissue damage. Interestingly, Casanova et al. [173] came to the opposite conclusion and found that the average rupture force and surface dimpling increased with increasing insertion speed. These contrasting findings may be caused by the different tissues used in these studies, particularly pig heart in [188] and rat brain in [173]. While the heart is more densely made up of cardiomyocytes, the brain is more viscous due to the high proportion of water. Furthermore, Casanova et al. [173] also compared the responses of brain-mimicking hydrogels and real brain tissue and found that hydrogels exhibited opposite trends for dimpling and friction stress with

insertion speed. In their study, Mahvash and Dupont [188] also examined the rupture transitions between tissue layers, which is important in brain tissue because the properties of GM and WM show significant differences [109].

These findings highlight the requirements for creating specialized brain-needle models that must further consider the heterogeneity and anisotropy of brain tissue. Experiments are essential for the development and validation of such models. While a small number of experiments have been conducted with brain tissue, *e.g.*, rat brain [173] and swine brain [178], most existing studies are based on tissue-mimicking materials [25,94,187,192].

At the initial stage of drug infusion, when the drug infusion rate is higher than the drainage rate, the retained drug fluid will generate a high hydraulic pressure at the tip of the needle and compress the local tissue forming a spherical cavity filled with drug fluid. Hydraulic pressure can also open and enlarge the gaps between the needle wall and the tissue, allowing fluid to flow back to the tissue surface. This is the so-called backflow, one of the main problems in CED treatment [173,193,194]. Because the high local pressure can potentially cause discomfort or other complications to the patient and the backflow would significantly reduce the drug volume, local tissue compression should be avoided.

The FSI modeling method is ideal for capturing the fluid-solid interface and helps in the development of backflow-free needles and procedures [193]. However, FSI has so far not been widely applied due to the numerical challenges of some factors, *e.g.*, (i) the fluid-solid interface is not constant but varies with hydraulic pressure, (ii) the fact that the tissue itself is permeable. Alternatively, [195] proposed using multiple layers of solid elements to represent the flow and tissue. The deformability of the two layers of solid elements enables capturing of the deformation of fluid-solid boundaries. This method was then adopted and extended to 3D by Orozco et al. [194]. The accuracy of this method highly depends on the properties of the solid elements, which must match the behavior of the fluid. Ivanchenko et al. [196] also applied the hydraulic pressure directly to the solid domain to solve the solid deformation. Particular attention must then be paid to the applied hydraulic pressure.

3.3. Development of hydrogels to mimic brain tissue

Because brain tissue is not easily accessible and raises ethical issues, synthetic materials that have similar mechanical properties to the real brain are gaining increasing attention [197]. As mentioned above, some needle-tissue studies are based on phantoms. Hydrogels are, among other materials, the most commonly used materials that can mimic the mechanical and hydraulic behavior of brain tissues. These properties allow the hydrogels to serve as phantoms and provide real-scale training models for developing treatments, *e.g.*, drug delivery, tumor resection and device implantation [198–200]. Reported brain-mimicking phantoms include those developed by Forte et al. [201,202] and Tan et al. [203] for brain surgery and drug delivery (among other things, the nonlinear mechanical properties of the brain-like hydrogel were fully characterized by Kainz et al. [204]), Lavrova et al. [205] for the study of molecule diffusion in the brain, Distler et al. [206] for various loading conditions, including compression, tension and torsional shear, and Vanina et al. [207] for modeling complex metabolic transport processes.

Researchers have also compared the properties of different materials against different tissues and loading conditions with the aim of finding solutions to further improve existing materials and also provide guidance on material selection. Leibinger et al. [208] concluded that while gelatin (a commonly used phantom [209]) reproduces well the needle insertion forces of the brain, a newly designed composite hydrogel developed at Imperial College [201] can better mimic the viscous nature of the soft tissue. Navarro-Lozoya et al. [210] compared hydrogels and emulsions with porcine brain tissue under similar strains and strain rates and concluded that the emulsion exhibits mechanical responses more similar to those of native porcine brain tissue than the other candidates. Tejo-Otero et al. [211] even tested a number of commonly used hydrogels (*e.g.*, agarose, polyvinyl alcohol -PVA-, Phytagel -PHY- and methacrylate gelatine -GelMA-) and compared their mechanical properties to a variety of organs (*e.g.*, liver, heart, kidney and brain) and drew some important practical conclusions.

With the remarkable advancement of 3D printing techniques for hydrogels [212], brain-like properties can be achieved at the macro scale by programming the microstructure of the material. This requires a quantitative understanding of the key microstructural factors that govern the macroscale properties, thus enabling precise microstructural design [213]. Dimensional analysis, as represented by the Buckingham π theorem, provides powerful tools for identifying the key dimensionless parameters that govern some specific physical phenomenon. For example, the well-known Reynolds number, known in fluid mechanics, regulates the flow patterns [214]; and a series of dimensionless parameters proposed by Yuan and colleagues can control the nonlinear buckling process [215–217]. Therefore, if the key dimensionless microstructural parameters that control the mechanical and hydraulic behavior of the brain can be identified, our ability to develop and program brain-mimicking phantoms will be greatly improved. The good news is that in recent years, machine learning has made complex dimensionless analyses more accessible [218,219].

3.4. Supporting techniques

To understand the mechanical behavior of brain tissue and characterize its mechanical properties, mechanical testing techniques are required. The most commonly used techniques are compression testing, (including confined compression, unconfined compression and indentation), tension testing and shear testing.

Indentation testing methods [220,221] are often used to characterize compression behavior and to develop constitutive models of brain tissue. Since compression is the most common deformation pattern of the brain, most mechanical tests of brain tissue have been performed using indentation methods, as summarized in Table 2. Brain tissues have been shown to be strain rate and depth sensitive materials [99,109,131], so strain rate and indentation depth are important factors to consider in these tests. In published data, strain rates used for brain tissue testing are up to 3000/s. Indentation tests can also be carried out at different scales. While macroscopic indentations extract the macroscale and homogenized properties of tissues for practical applications and modeling, microscopic indentations are able to capture localized properties to reveal some unknown mechanisms [110,127]. Furthermore, indentation testing can be performed *in vivo* and provide results with high fidelity [158,159].

Tensile testing is another type of mechanical testing used to determine mechanical properties of materials in which a controlled tension is applied to a sample until it fails. In fact, compared to indentation testing, it provides more comprehensive information about the mechanical properties of the material. However, since (i) this type of test is often used for materials that can withstand tensile forces without immediately breaking while brain tissue is extremely soft and vulnerable, (ii) a larger sample size is required while brain tissue is difficult to obatin, and (iii) it cannot be performed *in vivo* due to its destructive power, tension tests are relatively rarely used for mechanical tests of brain tissue (see Table 2). Nevertheless, Miller and Chinzei [99] showed that swine brain tissue was significantly softer when extended than when compressed, and the brain tissue constitutive models developed

based on compression experiments are not sufficient to explain tissue behavior under tension. Similarly, Eskandari et al. [166] observed that brain tissue exhibited strain-stiffening under compression and strain-softening under tension. Budday et al. [110] also concluded that material parameters of the human brain identified for a single loading mode cannot predict a response under arbitrary loading conditions. Therefore, tensile testing is essential to fully describe the mechanical behavior of brain tissue.

However, in terms of the drug-delivery process, tension is not the main pattern of tissue deformation. On the other hand, the shear deformation caused by needle insertion might be more relevant. Shear properties (*e.g.*, the shear modulus) of soft tissue can be measured by applying shear deformation and recording the reaction force, and there are a number of studies that have conducted shear tests with brain tissue [97,104,106,108,110,126,164]. It is worth noting that magnetic resonance elastography (MRE) is a new technique that can precisely measure the stiffness, shear moduli and viscosity of brain tissue *in vivo* [222–224]. The mechanism is to use a mechanical vibrator on the surface of the patient's body to generate shear waves that propagate into deeper tissues of the patient, measure the propagation and velocity of the waves using an MRI acquisition sequence, and finally map the stiffness using inversion algorithms. The resolution reaches the scale of mm ∼ cm [225]. However, since tissue stiffness is calculated by the inversion algorithm, the MRE measurements may be inaccurate for regions with strong heterogeneity, *i.e.* where the stiffness varies over a very small distance [226].

4. Solid mechanics: properties and deformation of neurons

4.1. Mechanical properties of neurons

At the cellular level, the neurons and their mechanical behavior also play an important role in brain drug delivery. On the one hand, neurons constitute the brain tissue, so their mechanical properties and spatial distribution directly determine the mechanical behavior of the brain tissue. On the other hand, the gaps between neurons form the fluid flow pathway, so their mechanical behavior can divert the drug delivery route. Consequently, a deep understanding of the mechanical response and properties of neurons is crucial for developing precise drug-delivery procedures in the brain and can also unravel some unsolved brain problems related to fluid and mass transport [37].

As mentioned in Section 1 and illustrated in Fig. 1, neurons consist of three parts: the cell body, also called the soma, which contains genetic information and maintains the structure of the neurons, and provides energy to drive activities; the axon, a long tail-like structure that connects to the cell body at a special junction, often insulated with a fatty substance called myelin that helps them transmit an electrical signal; and the dendrites, which are fibrous roots that branch off from the cell body and receive/process signals from the axons of other neurons. This slender structure makes neurons extremely soft and flexible, with the equivalent elastic moduli typically in the range of 0.1 ∼ 2 kPa [227]. This means that even minor mechanical stimulation may deform the neurons, while the drug infusion pressure can reach up to 10 kPa [5]. In addition, neurons also show hysteretic features, strong nonlinearity and significant time/rate dependencies [12,228]. Therefore, some hyper- and viscoelastic material models have been proposed and the corresponding parameters characterized to describe the mechanical behavior of neurons [12,13,228,229]. The fracture property of neurons is another important factor to be considered when injecting drugs as a benchmark for defining the threshold of locally applied hydraulic pressure. According to Hasan et al. [230], the failure strains for the microtubules and Tau proteins (major components of neuronal cytoskeleton) are 50 and 40%, respectively,

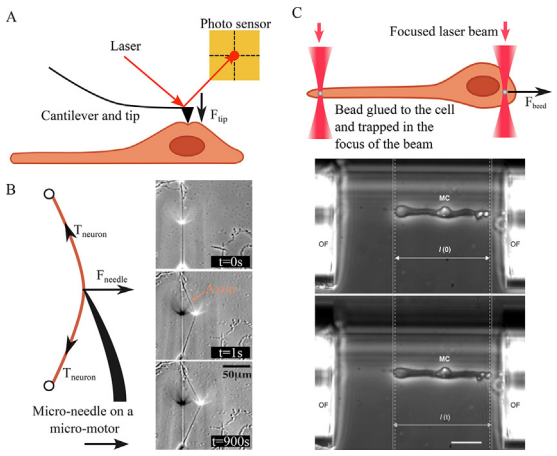

Fig. 7. Methods for measuring the mechanical properties of neurons: (A) Schematic representation of the indentation test using atomic force microscopy. (B) *Left*: Schematic representation of the tension test with micro-needle and micro-motor system. *Right*: Neuron deformation over time using the micro-needle and micro-motor system; reproduced from Bernal et al. [12]. (C) *Top*: Schematic representation of the tension test with optical tweezers. *Bottom*: Neuron stretch with and without applying optical tweezers; reproduced from Lu et al [229].

and the corresponding axonal failure strain and stress vary between 6 and 11% and 5 ∼ 19.8 MPa under strain rates from 10/s to 50/s. All the above evidence supports the need to consider the mechanical behavior of neurons to better capture the process of drug delivery in the brain.

4.2. Supporting techniques

The techniques that have been used to measure the mechanical properties of neurons can be categorized into indentation methods and tension methods, although all types of tests are very rare in the literature. The indentation method is mainly based on the use of atomic force microscopy (AFM). Using a very sharp tip attached to a cantilever, as shown in Fig. 7A, AFM is capable of not only scanning over a sample surface and restoring the shape of the surface, but also to penetrate the sample and return the force-displacement curve. Lu et al [229] used AFM to determine viscoelastic properties of neurons and glial cells from the mammalian brain (hippocampus) and retina. They found that elastic behavior dominates over viscous behavior in all CNS cells. Zhang et al. [231] used AFM to show that the stiffness of the axon plasma membrane is significantly higher than the stiffness of dendrites and soma using cultured rat hippocampus neurons. Regarding the tension test of neurons, Bernal et al. [12] used a micro-needle mounted on a direct current motor to retract the neurons like pulling back a bow, and recorded the force-displacement curve, as shown in Fig. 7B. They observed elastic response, viscoelastic relaxation and active contraction, and created a constitutive model to describe these behaviors. Optical tweezers/stretchers/trap, a type of technology that uses laser beams to manipulate microscopic and sub-microscopic objects, offers another approach to conducting tension testing on neurons, as shown in Fig. 7C, and has been widely used to study cell mechanics [232,233]. In the work by Lu et al. [229], the optical stretcher has also been used to measure the viscoelastic properties of glial cells and neurons. Other techniques such as the nano tensile tester [234] and the magnetic (electromagnetic) tweezers [235] could also offer alternatives. The theories, capabilities and limitations of these advanced, high-precision techniques are systematically reviewed by Neuman and Nagy [236]. A comprehensive analysis of neuronal biomechanics using AFM can also be found in [237].

In addition, understanding and modeling the behavior of neurons also requires ultra-high resolution imaging techniques to observe the components in neurons and reconstruct the geometry or microstructure of neurons to model them [227,230]. Using SEM, the cross-sectional view of the axons revealed the cytoskeleton of the axon, which includes the microtubules, Tau proteins, neurofilaments, and microfilaments, and that the microtubules are organized in a hexagonal arrangement and cross-linked by proteins [230]. Using FIB-SEM, Wu et al. [238] reconstructed the realistic 3D structure of neurons, and in addition, Bernardini et al. [239] built a comprehensive database of the size and shape distribution of axons in the ovine brain. These data allow researchers to reconstruct neurons and conduct numerical studies to gain a deeper understanding of the mechanical behaviors of neurons across scales [13].

5. Mathematical models for brain drug delivery

While biomechanics and biophysics focus on a few specific factors to build the principles that control the drug-delivery processes in the brain, mathematical models utilize these principles and integrate the information to further predict the entire drug-delivery process. Due to the flourishing biomechanical and biophysical research on the brain, numerous mathematical models for drug delivery in the brain have been proposed. Here, we focus primarily on infusion-based methods of drug delivery.

5.1. Single-phase models

As mentioned in Section 2, the convection-diffusion-reaction equation is a fundamental principle in building mathematical models for drug delivery. An example of seminal work dates back to 1997, when Kalyanasundaram et al. [15] used MR images to rebuild brain geometry in 2D. The employment of the convection-diffusion equation allowed them to simulate the interleukin-2 transport in the brain parenchyma post-ventricular perfusion and, based on the simulation results, identify the essential role of brain microstructure and drug transport properties on the delivery of this specific drug. A more advanced image-based brain model in 3D was set up years later, enabling the comparison of various brain regions [240]. Their study demonstrated the significant differences in drug distribution in the GM and WM, in particular along and perpendicular to axons, indicating the necessity to develop models that can consider tissue anisotropy and microstructural heterogeneity. Linninger et al. [16,20,30] and Kim et al. [31,241,242] developed a protocol and model to extract tissue anisotropy and heterogeneity from DTI images. Moreover, their drug delivery model was also developed with the capability of considering drug metabolism and elimination, including drug absorption, distribution, metabolism, and excretion (ADME). These contributions further increased the model's accuracy in predicting drug delivery in the brain and provided valuable references for optimizing the design of the CED infusion catheter. In pharmacology, the ADME processes of drugs can be mathematically described using pharmacokinetic models [17]. These models are particularly useful for understanding the fate of drugs in the brain and have therefore been widely developed and adopted.

The fluid field of drugs in brain tissue is also affected by other biofluids and components in the brain, such as CSF and ISF, which form other phases in mathematical models. Stine and Munson thoroughly analyzed the relationship between CED and ISF dynamics in their review [243]. A biphasic model, which is more systematic, was established by Linninger and colleagues by coupling pulsatile CSF motion with intracranial pressure [244,245]. Although the model was developed to investigate hydrocephalus and external fluid which was not considered, it could still be utilized to simulate drug delivery through CED. Later, a nonlinear biphasic model was further developed by considering fluid exchange between the blood and tissue. This allowed the model to represent a more complex system for cerebral flow infusion analysis [246]. To be closer to reality, ISF, blood plasma [247,248] and tumor leakage [249] were also considered in the following studies. In the mathematical models by Zhan and colleagues [18,19,29,32,44,250], multiple steps in brain drug delivery, including drug release and bioreactions, werecombined with the drug fluid and ISF. The Physiologically-based pharmacokinetics (PBPK) models have the advantage of providing more accurate and comprehensive results because they take into account the physiological and anatomical differences between individuals, such as blood flow rates between specific organs, tissue partitioning coefficients, and organ size [251–253]. Therefore, a number of other PBPK models are also being developed to predict the fate of different drugs in different brain compartments [254–259]. Readers can refer to a recent book chapter [260] and a review [261], in which the pharmacokinetic principles and anatomical connections of drug distribution in the brain have been comprehensively presented.

Since these models only consider the drug fluid, we categorize them as a type of single-phase model. By using advanced imaging techniques to create realistic geometries, single-phase models have become very sophisticated after almost 20 years of development. However, findings from biomechanical and biophysical studies clearly show that the drug-delivery process in the brain does not involve just one phase. The tissue and neuron deformations, for example, must be taken into account.

5.2. Considerations of the biphasic nature of the brain

The deformation of the neuron leads to microstructural deformation, which can alter the local flow field and trigger the development of biphasic models for the brain. Chen et al. [262] established one of the earliest poroelastic models of brain tissue in 2002 to enable the prediction of fluid flow in brain tissue in CED with improved accuracy. In addition to the possibility of visualizing the flow field in the brain, the tissue microstructure deformation caused by the localized fluid pressure could also be included in the model. To validate the model, brain-like agarose gel experiments were performed. As the first step to establish the poroelasticity model for the tissues of brain, some assumptions were introduced, particularly the tissue was considered linear elastic, isotropic and homogeneous. To relax the linear elastic assumption, Chen and Sarntinoranont [179] applied an exponential equation to describe the tissue deformation and hydraulic permeability, derived from agarose gels and biological tissues, *e.g.* cartilage. In addition to the application of empirical relations, the introduction of nonlinear material properties to the model is an effective way, which has already been studied in detail, particularly in Smith's group. They first utilized an Ogden-type hyperelastic compressible function to describe brain tissues, enabling modeling of the nonlinear relationship existing between local hydraulic permeability and local fluid pressure [180]. The later model which geometrical nonlinearity was added allowed simulation of the hydraulic permeability's dependence on both the matrix strain and nonlinear boundary conditions at the infusion cavity [263]. A comparison of modeling prediction from single-phase and biphasic models demonstrated the importance of considering the matrix's finite deformation when predicting drug concentration and its distribution pattern. Moreover, their studies also highlighted the necessity to experimentally determine the brain tissue's material nonlinearity in a range of strains [263,264].

Another potential improvement of poroelastic models is to include the anisotropy and heterogeneity of brain tissues. In pioneering work performed by Støverud et al. [265] in 2012, patient-specific brain structures and parameters were acquired from DTI

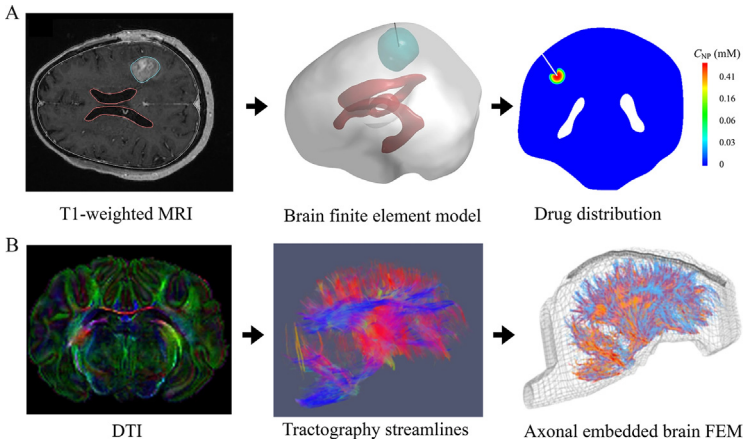

Fig. 8. Finite element models for the brain: (A) Finite element modeling for drug delivery in the brain. Brain geometry is reconstructed using magnetic resonance imaging (MRI); reproduced from Yang and Zhan [19]; C_{NP} stands for the drug concentration. (B) Registration of tissue anisotropy based on diffusion tensor imaging (DTI); reproduced from Hajiaghamemar et al. [269].

data and implemented into their biphasic model. The model characterized the difference between WM and GM in terms of fractional anisotropy, whereas, material nonlinearity was not covered. Despite widespread acceptance of accounting for the two-phase nature of the brain, the implementations at the whole brain level and in drug-delivery scenarios are scarcely seen.

Obviously, consideration of the biphasic nature of the brain highlights the importance of understanding and characterizing the hydraulic and mechanical properties of brain tissue and neurons, which have been discussed in Sections 2–4.

5.3. Supporting techniques and databases

Obviously, the mathematical model's development is inextricably linked to the development of imaging techniques and geometry reconstruction methods as well as the construction of experimental databases that can be used to validate the models.

Mathematical models are commonly established based on idealized geometrical models at the initial stages of development. For instance, Chen et al. [262] developed their poroelastic biphasic model in 2002 using brain phantom gels, which could be considered isotropic and homogeneous. The model was upgraded to include material and geometric nonlinearity while it was still based on an idealized model in spherical geometry [179,180,246,263,264,266]. Idealized models are suitable for conducting parametric scan to determine the impact of different materials and administration parameters on the spatial profile of drug concentration since geometric properties are not a primary focus. Hence, in recent years, the spherical model is still used to examine how drug diffusion anisotropy and tissue permeability determine the delivery outcome of CED [29]. Notably, so far, most simulation studies of drug particle diffusion are based on idealized models [26,266–268]. The main reasons are (i) the shortage of high-resolution and accurate anatomical images to re-build brain tumor microstructure; and (ii) the high requirement on computational resources and power to perform particle-tracking simulations that can accommodate the complex realistic tissue microstructure and micro-environment.

Given the importance of anisotropy and heterogeneity of brain tissues, more realistic geometric models are necessary to ensure the modeling prediction accuracy at the relevant length scales [29,270]. Anatomical MRI and DTI techniques have been extensively developed and applied in simulation studies in the last few years. In the earliest work done by Kalyanasundaram et al. [15] in 1997, a realistic 2D brain geometry was extracted from MRI data. This was closely followed by the reconstruction of the brain in 3D from anatomic MRI [270]. With the recognition of the importance of anisotropy, DTI technology has also begun to be widely used to characterize the orientation of neurons, particularly axons in WM [30]. Since then, the use of anatomical MRI and DTI techniques to reconstruct the brain, as shown in Fig. 8, has gradually become a conventional method in mathematical modeling applications [31,32,44,241,242,248,249,265]. The primary objective of developing mathematical models is to offer recommendations for preoperative planning. However, because of individual differences, a geometric model cannot be used for different patients. Therefore, the procurement of patient-specific models also become a hot topic and has been extensively studied [93,271–273]. As a practical diffusion MRI technique, Neurite Oriented Dispersion and Density Imaging (NODDI) can provide estimations of the microstructural complexity of dendrites and axons *in vivo* on clinical MRI scanners Zhang et al. [274]. Such detailed information on tissue

Table 3
Animal studies that can develop and improve mathematical models of drug delivery in the brain.

Subjects	Health condition	Infusion substance	Measured parameters	Images	Refs.
Monkey	Healthy	MRI contrast agent Gadoteridol	Infusate position and size, flow rate	MRI, DTI	[276]
Monkey	Healthy	liposomal GD, free GD	Flow rate, distribution of GDNF protein	MRI	[277]
Porcine	Healthy	MR marker Gadodiamide	Tracer concentration, flow rate, brain tissue expansion	MRI	[278]
Rat	Healthy	Gd-DTPA albumin tracer	Tracer distributions, flow rate	MRI, DTI	[31]
Monkey	Healthy	Saline	Flow rate, infusate distribution, anisotropy, and temporal dynamics, tissue structure change	MRI, DTI	[279]
Sheep	Healthy	Gadolinium (GD)	Flow rate, GD distribution	CBCT, MRI	[280]
Pig	Healthy	GD	Flow rate, GD distribution	MRI	[281]
Human	Brain tumor	Gd-DTPA tracer	Flow rate, distribution and concentration of Gd-DTPA tracer	MRI	[273]

microstructure can improve mathematical models. The most impressive feature in terms of mathematical modeling is its ability to provide *in vivo* information about the local porosity distribution. Since the hydraulic permeability of porous media is closely related to the porosity of the medium and the correlation of permeability with variable porosity is the basis of biphasic models, NODDI holds great potential to be an effective tool in further improving the mathematical modeling of drug delivery in the brain.

A number of animal studies of CED have been performed in swine, monkey, ovine, and rat models, and there are also some clinical trials with human patients. These experiments and trials are important databases that can be used to create and improve mathematical models of drug delivery in the brain. The detailed information of some referenced experiments is summarized in Table 3. Further preclinical and clinical evidence can be found in the review [275] and on ClinicalTrials.gov (a database of privately and publicly funded clinical studies conducted around the world).

6. Conclusions, challenges and perspectives

Mathematical models for infusion-based drug delivery in the brain have steadily improved over the past twenty years, particularly with the advancement of emerging supporting techniques. However, several gaps still need to be filled to meet clinical requirements. In this section, we first summarize the strategy for modeling infusion-based drug delivery in the brain, drawing on key findings from the reviewed studies. This will help readers get clear ideas of how to build proper models according to the needs of their search. We then highlight the major gaps in the development of next-generation models and provide insights into strategies to potentially address these gaps.

It is worth noting that although most of the studies reviewed relate to CED, the most representative type of mechanically controlled drug delivery in the brain, there are also other types, such as focused ultrasound blood-brain barrier disruption [282], which uses ultrasound waves to temporarily open the BBB to allow drugs to pass, and magnetic field-assisted drug delivery [283]. They also involve fluid transport and tissue deformation. Therefore, the insights of this article are also applicable to modeling other types of mechanically controlled drug delivery in the brain.

6.1. Summary

In this article, we have provided a comprehensive overview of the current status of the field to shed light on the development of a next-generation computational model that can accurately predict infusion-based drug delivery in the brain from physical, mechanical, and mathematical perspectives.

In general, the convection-diffusion-reaction Eq. (1), as discussed in Section 2, provides the framework for capturing the time-varying drug concentration distribution in the brain. The construction of this equation requires a number of inputs, namely tissue permeability, drug diffusivity and drug clearance rate, which can be characterized by methods discussed in Section 2.4. Due to the biphasic nature of the brain, the permeability of brain tissue varies during the drug transport process, as drug flow can deform the nerve cells and change the flow pathway, as shown in Fig. 4 [13,24]. This problem can be solved by adopting (i) a pressure-dependent permeability tensor for brain tissue, as developed by Yuan et al. [13] and (ii) the poro-elastic theory and computational models that connect tissue deformation with permeability change, as discussed in Sections 3.1.5 and 5.2, respectively. Capturing fluid-cell interactions at the cellular level is crucial for developing pressure-dependent permeability tensors and advanced poro-elastic models to more accurately predict drug delivery in the brain. Therefore, we discussed the properties of nerve cells in Section 4.

A complete model should also account for the effects of needle implantation and drug injection on the ability to administer drug delivery and thus be able to provide practical suggestions for conducting drug delivery. The needle implantation process can be modeled by properly describing the needle-brain interaction (*i.e.* friction, shear deformation, crack initiation, crack propagation). The process of drug injection, which involves the complex interactions that lead to tissue swelling and backflow (Fig. 5B and C), can potentially be modeled by FSI techniques and models [193]. However, modeling the backflow is still challenging, as analyzed in Section 3.2. The properties and constitutive models form the basis for modeling brain deformation during these processes, which were analyzed in detail in Section 3.

6.2. Limitations and future work in parameter identification

Parameter identification of processes governing drug delivery in the brain is currently highly variable. For example, the measured hydraulic permeability values of brain tissue differ by a factor of 1000 among different studies, as shown in Table 1. This can be attributed to differences in brain regions, species, measurement methods and environmental conditions, *etc*. It should be noted that sample preparations in these tests (*e.g.*, shipping, cutting) can have a significant effect on the hydraulic permeability since the microstructure of the porous medium would inevitably change. However, due to the limitations and possible biases in the experimental setups, as analyzed in Section 2.4.1, there are no gold standard methods. In addition, the current understanding of the mechanical properties of neurons is neither sufficient nor comprehensive, while abundant evidence demonstrates the significant influence of the mechanical behavior of neurons on drug delivery pathways in the brain. The question therefore arises as to how to develop gold standard methods to generally and precisely identify the properties that govern drug delivery in the brain, *e.g.*, the permeability tensor of brain tissue, the diffusivity tensor of drug particles, constitutive models of brain tissues and neurons are essential. Furthermore, the question of how to characterize these properties non-invasively is not currently addressed but, once resolved, would greatly contribute to clinical practice.

Alternatively, numerical modeling offers great potential to assist in the characterization of these properties, but the precision depends heavily on the fidelity of the microstructural description. Although the NODDI technique has made it possible to map the local porosity of the brain, additional details, *e.g.*, the neuron size distribution, are required to map the permeability tensor. There is also a need for models and techniques at the molecular and neuron scales that can help identify the interactions between neurons and drug molecules. This is not only valuable for the discovery of new efficient drugs, but can also provide information for establishing and improving upper-scale models.

6.3. Disease-induced alterations

The occurrence of pathologies can lead to changes in tissue microstructure, thereby affecting the results of drug delivery. On the one hand, parameters that reflect tissue properties can be changed significantly. For example, tissue permeability in brain tumors can become an order of magnitude higher than that of surrounding normal tissue due to increased tissue porosity and changes in the proportion of extracellular matrix components [284]. Moreover, tissue porosity varies with the grade of brain tumors [285,286], further expanding the spectrum of tissue permeability changes. These changes in tissue microstructure also complicate drug delivery. In neurodegenerative diseases, the change or loss of neuronal myelin

[287,288] can alter the surface charge of axons, which may further influence the outcomes of nanoparticle-mediated drug delivery due to the crucial role of Coulomb forces in determining nanoparticle diffusion in the brain tissue [27]. On the other hand, these alterations also affect model assumptions. For example, mathematical models of drug delivery to the brain often assume that BBB is intact. However, it has been found that intratumoral microvasculature can become leaky in metastatic brain tumors [289], making the assumption of an intact BBB less valid for simulating drug delivery to these tumors. The effects of disease on tissue properties are diverse and may be interrelated, ultimately affecting drug transport and accumulation. This influence may vary depending on the disease type, highlighting the need to establish disease-specific models.

6.4. Limitations and future work in modeling approaches

Drug delivery in the brain is a multiscale process and includes several phases. The final drug distribution pattern throughout the brain is determined by the underlying complex sub-processes down to the neuron and tissue scales, which are governed by interactions between different physical factors. Once the effects of individual phases have been identified, how to reconcile the interactions between these different phases (*i.e.* chemical reaction, biological metabolism, mechanical behavior) and different components (*e.g.*, ECM, neurons, ISF, CSF) in one equation system is also a challenging problem. Furthermore, the homogenization of this system of equations in the heterogeneous and anisotropic brain tissues still remains a challenge given the multiple scales.

At the tissue and brain scales, consolidation theory (*i.e.* poroelastic/poroviscoelastic models) is a great inspiration and a powerful tool to study the mechanical behavior of brain tissue during the drug infusion process. While the assumption that local homogeneity and isotropy agree well with geological experiments, the same hypothesis may not be applicable to brain tissues. To obtain more accurate outcomes, it is worth going to the microscopic scale to analyze the interaction between the hydraulic pressure and the microstructure, which also increases the need for a reconstruction method with higher resolution imaging techniques.

There is not enough research on how to capture the phenomena caused by the interactions between the drug and the brain tissue across scales. These include tissue swelling due to the accumulation of the drug at the needle tip, backflow (*i.e.* drug flow back along the gap between the needle wall and the tissue when the local hydraulic pressure is high), and tissue recovery due to the absorption and drainage of the drug, as shown in Fig. 5. Section 3.2 has reviewed studies on tissue needle interactions, but very few studies have involved brain tissue. The difficulty in modeling these phenomena lies in the continuously evolving fluid-solid interfaces. The pressure-dependent permeability of brain tissues due to the interaction between the fluid and neurons also requires more attention.

Model validation using experimental or clinical data, particularly at the brain level, represents an open challenge, mainly due to ethical issues and the lack of experimental/clinical data. Therefore, there are currently no fully validated computational models available to predict convection-enhanced drug delivery in the brain. In fact, as introduced in Section 5.3, some animal studies of CED have been conducted on swine, monkey, ovine, and rat models, and there are also some clinical trials on human patients, which are summarized in Table 3. These data could be used to validate brain-scale models. Model validation can focus on the outcomes of delivery, including the time course and spatial distribution of drug concentration, as well as treatment effectiveness, such as changes in tumor volume in cancer therapy.

6.5. Model-image compatibility and patient specificity

Currently, single-phase mathematical models have shown the best compatibility with advanced imaging-based digital brains, allowing them to assist clinical planning. However, a major shortcoming is that the role of tissue deformation in determining drug distribution cannot be taken into account. Although two-phase models can account for the coupling effects of fluid and solid phases, they have not yet been fully integrated into realistic geometric models. This may be attributed to numerical challenges and computational workload. Greater difficulties may arise when multiphasic mathematical models are solved on patient-specific brain structures, although this can significantly improve the reliability of the predictions. While searching for the most accurate method, one must also consider how to keep the trade-off between the advantages of advanced mathematical models and the heavy workload brought by realistic geometric models.

In addition, the biological and physiological properties of tissues as well as the transport properties of drugs can vary significantly from patient to patient and can be highly heterogeneous in some diseases, such as brain tumors. These variations and changes can greatly influence drug transport and accumulation, thereby affecting the outcomes of drug delivery. Advances in medical imaging techniques have enabled the interpretation of various tissue and drug properties from medical images of patients, which can be captured during diagnosis. The imaging protocols, tissue and drug properties, models for property extraction and applications for various modalities of MRI, CT, ultrasound and PET are discussed by Bhandari et al. [290]. Readers are encouraged to study Section 3 of this reference for detailed information.

6.6. Emerging technologies and approaches for improved drug delivery in the brain

Except for the infusion-based drug delivery method, emerging technologies have shown promise in overcoming the BBB in preclinical trials. Nano-sized drug delivery systems (DDSs) that encapsulate small molecular drugs with materials inert to bioreactions can effectively extend the circulation time and half-life of drugs in the human body [291], ensuring sustainable drug supply. In addition, surface modifications using specific ligands enable these DDSs to bind to corresponding receptors on the membrane of endothelial cells, thereby enhancing BBB penetration [292]. In addition, the combination of microbubbles and ultrasound was found to temporarily open the BBB [293]. Unlike most nano-sized DDSs that circulate throughout the body with the bloodstream, the location of BBB disruption can be precisely controlled by focusing ultrasound, allowing for more localized drug delivery to target regions in the brain. Beyond intravenous administration, CED offers an alternative by infusing drugs directly in the extracellular space of the tissue. To minimize tissue damage during catheter infusion, flexible catheters that can penetrate the tissue along a pre-designed trajectory have also been developed [294,295]. Their integration with an image-based path planner and visual navigation system can ensure accurate placement at the target infusion site while avoiding important and sensitive brain regions [95,296]. Limited drug penetration remains another challenge in brain drug delivery. Intravenously administered drugs accumulate mainly near capillaries [297], and the drug concentration in CED is high enough for effective therapy only near the infusion site [44,298]. Recent studies have demonstrated the potential to homogenize drug distribution using external magnetic fields [299]. Drug delivering through the glymphatic system [300] and intrathecal injection [301] also play prominent roles in the field of brain drug delivery. These techniques allow the drugs to transport though the convection of CSF, thus proving other ways to bypass the BBB. However, there

are significant challenges to be addressed before achieving their clinical applications. Therefore, they also require attentions to be paid to the specific processes, challenges, and solutions. Artificial intelligence (AI), with its powerful data processing capabilities, holds great potential in drug development and design to identify the most effective therapeutic compounds [302,303]. AI can also quickly extract tissue properties from medical images, providing a more detailed description of the patient-specific environment *in vivo* [304]. Since the patient's condition can change during treatment, reinforcement learning-based models have been developed to adapt drug delivery regimens in real time to the patient's evolving condition [305,306].

Declaration of competing interest

The authors declare that they have no known competing financial interests or personal relationships that could have appeared to influence the work reported in this paper.

CRediT authorship contribution statement

Tian Yuan: Writing – review & editing, Writing – original draft, Methodology, Investigation, Data curation, Conceptualization. **Wenbo Zhan:** Writing – review & editing, Writing – original draft, Methodology, Data curation. **Michele Terzano:** Writing – review & editing, Writing – original draft, Methodology. **Gerhard A. Holzapfel:** Writing – review & editing, Supervision, Methodology. **Daniele Dini:** Writing – review & editing, Supervision, Resources, Project administration, Methodology, Conceptualization.

Acknowledgements

This project has received funding from the European Unions Horizon 2020 research and innovation program under Grant Agreement No. 688279. Daniele Dini would like to acknowledge the support received from the EPSRC under the Established Career Fellowship Grant No. EP/N025954/1, the Shell/RAEng Research Chair in Complex Engineering Interfaces (RCSRF2122-14-143), and the Medical Research Council (MR/Y008448/1). Tian Yuan would like to acknowledge the support received from Great Britain-China Educational Trust award and the Medical Research Council (MR/Y008448/1).

References

[1] V.L. Feigin, T. Vos, E. Nichols, M.O. Owolabi, W.M. Carroll, M. Dichgans, G. Deuschl, P. Parmar, M. Brainin, C. Murray, The global burden of neurological disorders: translating evidence into policy, Lancet Neurol. 19 (3) (2020) 255–265, doi:10.1016/S1474-4422(19)30411-9.

[2] V.L. Feigin, E. Nichols, T. Alam, M.S. Bannick, et al., Global, regional, and national burden of neurological disorders, 1990–2016: a systematic analysis for the Global Burden of Disease Study 2016, Lancet Neurol. 18 (5) (2019) 459–480, doi:10.1016/S1474-4422(18)30499-X.

[3] N.J. Abbott, A.A.K. Patabendige, D.E.M. Dolman, S.R. Yusof, D.J. Begley, Structure and function of the blood–brain barrier, Neurobiol. Dis. 37 (1) (2010) 13–25, doi:10.1016/j.nbd.2009.07.030.

[4] A.M. Mehta, A.M. Sonabend, J.N. Bruce, Convection-enhanced delivery, Neurotherapeutics 14 (2) (2017) 358–371, doi:10.1007/s13311-017-0520-4.

[5] R.H. Bobo, D.W. Laske, A. Akbasak, P.F. Morrison, R.L. Dedrick, E.H. Oldfield, Convection-enhanced delivery of macromolecules in the brain, Proc. Natl. Acad. Sci. U.S.A. 91 (6) (1994) 2076–2080, doi:10.1073/pnas.91.6.2076.

[6] A. Jamal, T. Yuan, S. Galvan, A. Castellano, M. Riva, R. Secoli, A. Falini, L. Bello, F. Rodriguez y. Baena, D. Dini, Insights into infusion-based targeted drug delivery in the brain: perspectives, challenges and opportunities, Int. J. Mol. Sci. 23 (6) (2022) 3139, doi:10.3390/ijms23063139.

[7] J.H. Sampson, G. Archer, C. Pedain, E. Wembacher-Schröder, M. Westphal, S. Kunwar, M.A. Vogelbaum, A. Coan, J.E. Herndon, R. Raghavan, M.L. Brady, D.A. Reardon, A.H. Friedman, H.S. Friedman, M.I. Rodríguez-Ponce, S.M. Chang, S. Mittermeyer, D. Croteau, R.K. Puri, Poor drug distribution as a possible explanation for the results of the PRECISE trial: clinical article, J. Neurosurg. 113 (2) (2010) 301–309, doi:10.3171/2009.11.JNS091052.

[8] M.F. Salvatore, Y. Ai, B. Fischer, A.M. Zhang, R.C. Grondin, Z. Zhang, G.A. Gerhardt, D.M. Gash, Point source concentration of GDNF may explain failure of phase II clinical trial, Exp. Neurol. 202 (2) (2006) 497–505, doi:10.1016/j.expneurol.2006.07.015.

[9] F. Casanova, P.R. Carney, M. Sarntinoranont, Effect of needle insertion speed on tissue injury, stress, and backflow distribution for convection-enhanced delivery in the rat brain, PLoS One 9 (4) (2014) e94919, doi:10.1371/journal.pone.0094919.

[10] R.J. Mackenzie, Gray matter vs white matter, Neurosci. Technol. Netw. (2023). https://www.technologynetworks.com/neuroscience/articles/gray-matter-vs-white-matter-322973

[11] D.F. Meaney, Relationship between structural modeling and hyperelastic material behavior: application to CNS white matter, Biomech. Model. Mechanobiol. 1 (4) (2003) 279–293, doi:10.1007/s10237-002-0020-1.

[12] R. Bernal, P.A. Pullarkat, F. Melo, Mechanical properties of axons, Phys. Rev. Lett. 99 (1) (2007) 018301, doi:10.1103/PhysRevLett.99.018301.

[13] T. Yuan, W. Zhan, D. Dini, Linking fluid-axons interactions to the macroscopic fluid transport properties of the brain, Acta Biomater. 160 (2023) 152–163, doi:10.1016/j.actbio.2023.02.010.

[14] S. Ito, M. Funaoka, I. Hanasaki, S. Takei, M. Morimoto, M. Irie, H. Miyasaka, Visualization of the microstructure and the position-dependent diffusion coefficient in a blended polymer solid using photo-activation localization microscopy combined with single-molecule tracking based on one-color fluorescence-switching of diarylethene, Polym. Chem. 13 (6) (2022) 736–740, doi:10.1039/D1PY01100F.

[15] S. Kalyanasundaram, V.D. Calhoun, K.W. Leong, A finite element model for predicting the distribution of drugs delivered intracranially to the brain, Am. J. Physiol. Regul. Integr. Comp. Physiol. (1997). https://journals.physiology.org/doi/full/10.1152/ajpregu.1997.273.5.R1810

[16] A.A. Linninger, M.R. Somayaji, M. Mekarski, L. Zhang, Prediction of convection-enhanced drug delivery to the human brain, J. Theor. Biol. 250 (1) (2008) 125–138, doi:10.1016/j.jtbi.2007.09.009.

[17] W. Zhan, M. Alamer, X.Y. Xu, Computational modelling of drug delivery to solid tumour: understanding the interplay between chemotherapeutics and biological system for optimised delivery systems, Adv. Drug Deliv. Rev. 132 (2018) 81–103, doi:10.1016/j.addr.2018.07.013.

[18] W. Zhan, Convection enhanced delivery of anti-angiogenic and cytotoxic agents in combination therapy against brain tumour, Eur. J. Pharm. Sci. 141 (2020) 105094, doi:10.1016/j.ejps.2019.105094.

[19] Y. Yang, W. Zhan, Role of tissue hydraulic permeability in convection-enhanced delivery of nanoparticle-encapsulated chemotherapy drugs to brain tumour, Pharm. Res. 39 (5) (2022) 877–892, doi:10.1007/s11095-022-03261-7.

[20] M.R. Somayaji, M. Xenos, L. Zhang, M. Mekarski, A.A. Linninger, Systematic design of drug delivery therapies, Comput. Chem. Eng. 32 (1) (2008) 89–98, doi:10.1016/j.compchemeng.2007.06.014.

[21] J. Siepmann, F. Siepmann, A.T. Florence, Local controlled drug delivery to the brain: mathematical modeling of the underlying mass transport mechanisms, Int. J. Pharm. 314 (2) (2006) 101–119, doi:10.1016/j.ijpharm.2005.07.027.

[22] M. Vidotto, D. Botnariuc, E. De Momi, D. Dini, A computational fluid dynamics approach to determine white matter permeability, Biomech. Model. Mechanobiol. 18 (4) (2019) 1111–1122, doi:10.1007/s10237-019-01131-7.

[23] T. Yuan, W. Zhan, A. Jamal, D. Dini, On the microstructurally driven heterogeneous response of brain white matter to drug infusion pressure, Biomech. Model. Mechanobiol. 21 (4) (2022) 1299–1316, doi:10.1007/s10237-022-01592-3.

[24] A. Jamal, M.T. Mongelli, M. Vidotto, M. Madekurozwa, A. Bernardini, D.R. Overby, E. De Momi, F. Rodriguez y Baena, J.M. Sherwood, D. Dini, Infusion mechanisms in brain white matter and their dependence on microstructure: an experimental study of hydraulic permeability, IEEE Trans. Biomed. Eng. 68 (4) (2021) 1229–1237, doi:10.1109/TBME.2020.3024117.

[25] M. Terzano, D. Dini, F. Rodriguez y. Baena, A. Spagnoli, M. Oldfield, An adaptive finite element model for steerable needles, Biomech. Model. Mechanobiol. 19 (5) (2020) 1809–1825, doi:10.1007/s10237-020-01310-x.

[26] D. Su, R. Ma, M. Salloum, L. Zhu, Multi-scale study of nanoparticle transport and deposition in tissues during an injection process, Med. Biol. Eng. Comput. 48 (9) (2010) 853–863, doi:10.1007/s11517-010-0615-0.

[27] T. Yuan, L. Gao, W. Zhan, D. Dini, Effect of particle size and surface charge on nanoparticles diffusion in the brain white matter, Pharm. Res. 39 (4) (2022) 767–781, doi:10.1007/s11095-022-03222-0.

[28] M. Vidotto, A. Bernardini, M. Trovatelli, E. De Momi, D. Dini, On the microstructural origin of brain white matter hydraulic permeability, Proc. Natl. Acad. Sci. U.S.A. 118 (36) (2021), doi:10.1073/pnas.2105328118.e2105328118

[29] W. Zhan, F. Rodriguez y. Baena, D. Dini, Effect of tissue permeability and drug diffusion anisotropy on convection-enhanced delivery, Drug Deliv. 26 (1) (2019) 773–781, doi:10.1080/10717544.2019.1639844.

[30] A.A. Linninger, M.R. Somayaji, T. Erickson, X. Guo, R.D. Penn, Computational methods for predicting drug transport in anisotropic and heterogeneous brain tissue, J. Biomech. 41 (10) (2008) 2176–2187, doi:10.1016/j.jbiomech.2008.04.025.

[31] J.H. Kim, G.W. Astary, S. Kantorovich, T.H. Mareci, P.R. Carney, M. Sarntinoranont, Voxelized Computational model for convection-enhanced delivery in the rat ventral hippocampus: comparison with in vivo MR experimental studies, Ann. Biomed. Eng. 40 (9) (2012) 2043–2058, doi:10.1007/s10439-012-0566-8.

[32] W. Zhan, C.-H. Wang, Convection enhanced delivery of liposome encapsulated doxorubicin for brain tumour therapy, J. Controlled Release 285 (2018) 212–229, doi:10.1016/j.jconrel.2018.07.006.
[33] S. Budday, T.C. Ovaert, G.A. Holzapfel, P. Steinmann, E. Kuhl, Fifty shades of brain: a review on the mechanical testing and modeling of brain tissue, Arch. Comput. Methods Eng. 27 (4) (2020) 1187–1230, doi:10.1007/s11831-019-09352-w.
[34] S. Chatelin, A. Constantinesco, R. Willinger, Fifty years of brain tissue mechanical testing: from in vitro to in vivo investigations, Biorheology 47 (5-6) (2010) 255–276, doi:10.3233/BIR-2010-0576.
[35] A. Goriely, M.G.D. Geers, G.A. Holzapfel, J. Jayamohan, A. Jérusalem, S. Sivaloganathan, W. Squier, J.A.W. van Dommelen, S. Waters, E. Kuhl, Mechanics of the brain: perspectives, challenges, and opportunities, Biomech. Model. Mechanobiol. 14 (5) (2015) 931–965, doi:10.1007/s10237-015-0662-4.
[36] M.I. Khan, F. Hasan, K.A.H.A. Mahmud, A. Adnan, Recent computational approaches on mechanical behavior of axonal cytoskeletal components of neuron: a brief review, Multiscale Sci. Eng. 2 (4) (2020) 199–213, doi:10.1007/s42493-020-00043-4.
[37] M.K. Rasmussen, H. Mestre, M. Nedergaard, Fluid transport in the brain, Physiol. Rev. (2022). https://journals.physiology.org/doi/full/10.1152/physrev.00031.2020
[38] S.P. Neuman, Theoretical derivation of Darcy's law, Acta Mech. 25 (3) (1977) 153–170, doi:10.1007/BF01376989.
[39] S. Whitaker, Flow in porous media I: a theoretical derivation of Darcy's law, Transp. Porous Media 1 (1) (1986) 3–25, doi:10.1007/BF01036523.
[40] F.J. Suárez-Grau, Theoretical derivation of Darcy's law for fluid flow in thin porous media, Math. Nachr. 295 (3) (2022) 607–623, doi:10.1002/mana.202000184.
[41] T. Nagashima, N. Tamaki, S. Matsumoto, B. Horwitz, Y. Seguchi, Biomechanics of hydrocephalus: a new theoretical model, Neurosurgery 21 (6) (1987) 898–904.
[42] T. Nagashima, T. Shirakuni, S.I. Rapoport, A two-dimensional, finite element analysis of vasogenic brain edema, Neurologia Medico-Chirurgica 30 (1) (1990) 1–9.
[43] K.H. Rosenbluth, J.F. Eschermann, G. Mittermeyer, R. Thomson, S. Mittermeyer, K.S. Bankiewicz, Analysis of a simulation algorithm for direct brain drug delivery, Neuroimage 59 (3) (2012) 2423–2429, doi:10.1016/j.neuroimage.2011.08.107.
[44] W. Zhan, C.-H. Wang, Convection enhanced delivery of chemotherapeutic drugs into brain tumour, J. Controlled Release 271 (2018) 74–87, doi:10.1016/j.jconrel.2017.12.020.
[45] G.E. Kapellos, T.S. Alexiou, Chapter 1 - Modeling momentum and mass transport in cellular biological media: from the molecular to the tissue scale, in: Transport in Biological Media, Elsevier, Walthm, MA, USA, 2013, pp. 1–40, doi:10.1016/B978-0-12-415824-5.00001-1.
[46] E.A. Swabb, J. Wei, P.M. Gullino, Diffusion and convection in normal and neoplastic tissues, Cancer Res. 34 (10) (1974) 2814–2822. https://aacrjournals.org/cancerres/article/34/10/2814/479947/Diffusion-and-Convection-in-Normal-and-Neoplastic
[47] P.A. Netti, D.A. Berk, M.A. Swartz, A.J. Grodzinsky, R.K. Jain, Role of extracellular matrix assembly in interstitial transport in solid tumors, Cancer Res. 60 (9) (2000) 2497–2503. https://aacrjournals.org/cancerres/article/60/9/2497/507280/Role-of-Extracellular-Matrix-Assembly-in
[48] G. Franceschini, D. Bigoni, P. Regitnig, G.A. Holzapfel, Brain tissue deforms similarly to filled elastomers and follows consolidation theory, J. Mech. Phys. Solids 54 (12) (2006) 2592–2620, doi:10.1016/j.jmps.2006.05.004.
[49] T. Yuan, L. Shen, D. Dini, Porosity-permeability tensor relationship of closely and randomly packed fibrous biomaterials and biological tissues: application to the brain white matter, Acta Biomater. 173 (2024) 123–134, doi:10.1016/j.actbio.2023.11.007.
[50] A. Fick, V. On liquid diffusion, London Edinb. Dublin Philos. Magaz. J. Sci. 10 (63) (1855) 30–39, doi:10.1080/14786445508641925.
[51] B. Serin, R.T. Ellickson, Determination of diffusion coefficients, J. Chem. Phys. 9 (10) (1941) 742–747, doi:10.1063/1.1750834.
[52] C. Andrade, Calculation of chloride diffusion coefficients in concrete from ionic migration measurements, Cem. Concr. Res. 23 (3) (1993) 724–742, doi:10.1016/0008-8846(93)90023-3.
[53] T. Sasaki, Y. Gunji, T. Iida, Transient-diffusion measurements of radon: Fick's law confirmation and 218Po/214Po behavior determination, J. Nucl. Sci. Technol. 44 (10) (2007) 1330–1336, doi:10.1080/18811248.2007.9711379.
[54] M.P. di Cagno, F. Clarelli, J. Våbenø, C. Lesley, S.D. Rahman, J. Cauzzo, E. Franceschinis, N. Realdon, P.C. Stein, Experimental determination of drug diffusion coefficients in unstirred aqueous environments by temporally resolved concentration measurements, Mol. Pharm. 15 (4) (2018) 1488–1494, doi:10.1021/acs.molpharmaceut.7b01053.
[55] C. Nicholson, Interaction between diffusion and Michaelis-Menten uptake of dopamine after iontophoresis in striatum, Biophys. J. 68 (5) (1995) 1699–1715, doi:10.1016/S0006-3495(95)80348-6.
[56] C. Nicholson, K.C. Chen, S. Hrabětová, L. Tao, Diffusion of molecules in brain extracellular space: theory and experiment, in: Progress in Brain Research, volume 125, Elsevier, Walthm, MA, USA, 2000, pp. 129–154, doi:10.1016/S0079-6123(00)25007-3.
[57] D. Calvetti, Y. Cheng, E. Somersalo, A spatially distributed computational model of brain cellular metabolism, J. Theor. Biol. 376 (2015) 48–65, doi:10.1016/j.jtbi.2015.03.037.
[58] E. Vendel, V. Rottschäfer, E.C.M. de Lange, The need for mathematical modelling of spatial drug distribution within the brain, Fluids Barriers CNS 16 (1) (2019) 1–33, doi:10.1186/s12987-019-0133-x.
[59] X.-Y. Zhang, J. Luck, M.W. Dewhirst, F. Yuan, Interstitial hydraulic conductivity in a fibrosarcoma, Am. J. Physiol.-Heart Circ. Physiol. (2000), doi:10.1152/ajpheart.2000.279.6.H2726.
[60] P. Heneghan, P.E. Riches, Determination of the strain-dependent hydraulic permeability of the compressed bovine nucleus pulposus, J. Biomech. 41 (4) (2008) 903–906, doi:10.1016/j.jbiomech.2007.11.014.
[61] K.L. Kleinhans, A.R. Jackson, Hydraulic permeability of meniscus fibrocartilage measured via direct permeation: effects of tissue anisotropy, water volume content, and compressive strain, J. Biomech. 72 (2018) 215–221, doi:10.1016/j.jbiomech.2018.03.011.
[62] A.C.R. Tavner, T.D. Roy, K.W.W. Hor, M. Majimbi, G.R. Joldes, A. Wittek, S. Bunt, K. Miller, On the appropriateness of modelling brain parenchyma as a biphasic continuum, J. Mech. Behav. Biomed. Mater. 61 (2016) 511–518, doi:10.1016/j.jmbbm.2016.04.010.
[63] S. Cheng, L.E. Bilston, Unconfined compression of white matter, J. Biomech. 40 (1) (2007) 117–124, doi:10.1016/j.jbiomech.2005.11.004.
[64] L. Su, M. Wang, J. Yin, F. Ti, J. Yang, C. Ma, S. Liu, T.J. Lu, Distinguishing poroelasticity and viscoelasticity of brain tissue with time scale, Acta Biomater. 155 (2023) 423–435, doi:10.1016/j.actbio.2022.11.009.
[65] Y. Boucher, C. Brekken, P.A. Netti, L.T. Baxter, R.K. Jain, Intratumoral infusion of fluid: estimation of hydraulic conductivity and implications for the delivery of therapeutic agents, Br. J. Cancer 78 (1998) 1442–1448, doi:10.1038/bjc.1998.705.
[66] A.M. Saaibi, M. Sarntinoranont, An infusion and pressure system to measure hydraulic conductivity at a microscale level, ASME Digit. Collect. (2014) 561–562, doi:10.1115/SBC2008-193011.
[67] P. Shrestha, B. Stoeber, Imaging fluid injections into soft biological tissue to extract permeability model parameters, Phys. Fluids 32 (1) (2020), doi:10.1063/1.5131488.
[68] L. Su, J.-C. Lei, Z. Li, C. Ma, S. Liu, Wettability effect on hydraulic permeability of brain white matter, Acta Mech. Sin. 40 (2) (2024) 1–15, doi:10.1007/s10409-023-23278-x.
[69] C. Nicholson, L. Tao, Hindered diffusion of high molecular weight compounds in brain extracellular microenvironment measured with integrative optical imaging, Biophys. J. 65 (6) (1993) 2277–2290, doi:10.1016/S0006-3495(93)81324-9.
[70] R.G. Thorne, C. Nicholson, In vivo diffusion analysis with quantum dots and dextrans predicts the width of brain extracellular space, Proc. Natl. Acad. Sci. U.S.A. 103 (14) (2006) 5567–5572, doi:10.1073/pnas.0509425103.
[71] E.A. Nance, G.F. Woodworth, K.A. Sailor, T.-Y. Shih, Q. Xu, G. Swaminathan, D. Xiang, C. Eberhart, J. Hanes, A dense poly(ethylene glycol) coating improves penetration of large polymeric nanoparticles within brain tissue, Sci. Transl. Med. 4 (149) (2012) 149ra119, doi:10.1126/scitranslmed.3003594.
[72] J.J. Lochhead, R.G. Thorne, Intranasal delivery of biologics to the central nervous system, Adv. Drug Deliv. Rev. 64 (7) (2012) 614–628, doi:10.1016/j.addr.2011.11.002.
[73] S. Quader, K. Kataoka, H. Cabral, Nanomedicine for brain cancer, Adv. Drug Deliv. Rev. 182 (2022) 114115, doi:10.1016/j.addr.2022.114115.
[74] G. Ringstad, L.M. Valnes, A.M. Dale, A.H. Pripp, S.-A.S. Vatnehol, K.E. Emblem, K.-A. Mardal, P.K. Eide, Brain-wide glymphatic enhancement and clearance in humans assessed with MRI, JCI Insight 3 (13) (2018), doi:10.1172/jci.insight.121537.
[75] C.D. Arvanitis, G.B. Ferraro, R.K. Jain, The blood–brain barrier and blood–tumour barrier in brain tumours and metastases, Nat. Rev. Cancer 20 (2020) 26–41, doi:10.1038/s41568-019-0205-x.
[76] L.M. Valnes, S.K. Mitusch, G. Ringstad, P.K. Eide, S.W. Funke, K.-A. Mardal, Apparent diffusion coefficient estimates based on 24 hours tracer movement support glymphatic transport in human cerebral cortex, Sci. Rep. 10 (1) (2020) 1–12, doi:10.1038/s41598-020-66042-5.
[77] T. Yuan, Y. Yang, W. Zhan, D. Dini, Mathematical optimisation of magnetic nanoparticle diffusion in the brain white matter, Int. J. Mol. Sci. 24 (3) (2023) 2534, doi:10.3390/ijms24032534.
[78] X. Shi, A. von dem Bussche, R.H. Hurt, A.B. Kane, H. Gao, Cell entry of one-dimensional nanomaterials occurs by tip recognition and rotation, Nat. Nanotechnol. 6 (2011) 714–719, doi:10.1038/nnano.2011.151.
[79] X. Zhang, G. Ma, W. Wei, Simulation of nanoparticles interacting with a cell membrane: probing the structural basis and potential biomedical application, NPG Asia Mater. 13 (52) (2021) 1–18, doi:10.1038/s41427-021-00320-0.
[80] C. Manzo, M.F. Garcia-Parajo, A review of progress in single particle tracking: from methods to biophysical insights, Rep. Prog. Phys. 78 (12) (2015) 124601, doi:10.1088/0034-4885/78/12/124601.
[81] T. Kuhn, J. Hettich, R. Davtyan, J.C.M. Gebhardt, Single molecule tracking and analysis framework including theory-predicted parameter settings, Sci. Rep. 11 (9465) (2021) 1–12, doi:10.1038/s41598-021-88802-7.
[82] A.J. Onetto, S. Sharif, Drug Distribution, StatPearls Publishing, 2022. https://www.ncbi.nlm.nih.gov/books/NBK567736
[83] X. Lin, Y. Li, N. Gu, Nanoparticle's size effect on its translocation across a lipid bilayer: a molecular dynamics simulation, J. Comput. Theor. Nanosci. 7 (1) (2010) 269–276, doi:10.1166/jctn.2010.1358.
[84] T. Yue, X. Zhang, Molecular understanding of receptor-mediated membrane responses to ligand-coated nanoparticles, Soft Matter 7 (19) (2011) 9104–9112, doi:10.1039/C1SM05398A.

[85] C. Montis, D. Maiolo, I. Alessandri, P. Bergese, D. Berti, Interaction of nanoparticles with lipid membranes: a multiscale perspective, Nanoscale 6 (12) (2014) 6452–6457, doi:10.1039/C4NR00838C.
[86] C. Huang, Y. Zhang, H. Yuan, H. Gao, S. Zhang, Role of nanoparticle geometry in endocytosis: laying down to stand up, Nano Lett. 13 (9) (2013) 4546–4550, doi:10.1021/nl402628n.
[87] Y. Li, X. Chen, N. Gu, Computational investigation of interaction between nanoparticles and membranes: hydrophobic/hydrophilic effect, J. Phys. Chem. B 112 (51) (2008) 16647–16653, doi:10.1021/jp8051906.
[88] H.-m. Ding, Y.-q. Ma, Interactions between Janus particles and membranes, Nanoscale 4 (4) (2012) 1116–1122, doi:10.1039/C1NR11425E.
[89] K.B. Walhovd, H. Johansen-Berg, R.T. Káradóttir, Unraveling the secrets of white matter – bridging the gap between cellular, animal and human imaging studies, Neuroscience 276 (2014) 2–13, doi:10.1016/j.neuroscience.2014.06.058.
[90] R.I. Koning, A.J. Koster, T.H. Sharp, Advances in cryo-electron tomography for biology and medicine, Anna. Anatomy Anatomischer Anz. 217 (2018) 82–96, doi:10.1016/j.aanat.2018.02.004.
[91] M. Kleinnijenhuis, E. Johnson, J. Mollink, S. Jbabdi, K.L. Miller, A semi-automated approach to dense segmentation of 3D white matter electron microscopy, bioRxiv (2020).
[92] L. Vásárhelyi, Z. Kónya, Á. Kukovecz, R. Vajtai, Microcomputed tomography–based characterization of advanced materials: a review, Mater. Today Adv. 8 (2020) 100084, doi:10.1016/j.mtadv.2020.100084.
[93] E.D. Bander, K. Tizi, E. Wembacher-Schroeder, R. Thomson, M. Donzelli, E. Vasconcellos, M.M. Souweidane, Deformational changes after convection-enhanced delivery in the pediatric brainstem, Neurosurg. Focus 48 (1) (2020) E3, doi:10.3171/2019.10.FOCUS19679.
[94] S. Misra, K.B. Reed, B.W. Schafer, K.T. Ramesh, A.M. Okamura, Mechanics of flexible needles robotically steered through soft tissue, Int. J. Rob. Res. 29 (13) (2010) 1640–1660, doi:10.1177/0278364910369714.
[95] R. Secoli, E. Matheson, M. Pinzi, S. Galvan, A. Donder, T. Watts, M. Riva, D.D. Zani, L. Bello, F.R.y. Baena, Modular robotic platform for precision neurosurgery with a bio-inspired needle: System overview and first in-vivo deployment, PLoS One 17 (10) (2022) e0275686, doi:10.1371/journal.pone.0275686.
[96] A. Goriely, M.G.D. Geers, G.A. Holzapfel, J. Jayamohan, A. Jérusalem, S. Sivaloganathan, W. Squier, J.A.W. van Dommelen, S. Waters, E. Kuhl, Mechanics of the brain: perspectives, challenges, and opportunities, Biomech. Model. Mechanobiol. 14 (5) (2015) 931–965, doi:10.1007/s10237-015-0662-4.
[97] B. Rashid, M. Destrade, M.D. Gilchrist, Mechanical characterization of brain tissue in simple shear at dynamic strain rates, J. Mech. Behav. Biomed. Mater. 28 (2013) 71–85, doi:10.1016/j.jmbbm.2013.07.017.
[98] S.N. Sundaresh, J.D. Finan, B.S. Elkin, C. Lee, J. Xiao, B. Morrison, Viscoelastic characterization of porcine brain tissue mechanical properties under indentation loading, Brain Multiphys. 2 (2021) 100041, doi:10.1016/j.brain.2021.100041.
[99] K. Miller, K. Chinzei, Mechanical properties of brain tissue in tension, J. Biomech. 35 (4) (2002) 483–490, doi:10.1016/s0021-9290(01)00234-2.
[100] M. Kohandel, S. Sivaloganathan, G. Tenti, J.M. Drake, The constitutive properties of the brain parenchyma Part 1. Strain energy approach, Med. Eng. Phys. 28 (5) (2006) 449–454, doi:10.1016/j.medengphy.2005.01.005.
[101] A.E. Forte, S.M. Gentleman, D. Dini, On the characterization of the heterogeneous mechanical response of human brain tissue, Biomech. Model. Mechanobiol. 16 (3) (2017) 907–920, doi:10.1007/s10237-016-0860-8.
[102] A.M. Felfelian, A. Baradaran Najar, R. Jafari Nedoushan, H. Salehi, Determining constitutive behavior of the brain tissue using digital image correlation and finite element modeling, Biomech. Model. Mechanobiol. 18 (6) (2019) 1927–1945, doi:10.1007/s10237-019-01186-6.
[103] K. Miller, Constitutive model of brain tissue suitable for finite element analysis of surgical procedures, J. Biomech. 32 (5) (1999) 531–537, doi:10.1016/S0021-9290(99)00010-X.
[104] K. Laksari, M. Shafieian, K. Darvish, Constitutive model for brain tissue under finite compression, J. Biomech. 45 (4) (2012) 642–646, doi:10.1016/j.jbiomech.2011.12.023.
[105] A. Awasthi, U. Gautam, S. Bhaskar, S. Roy, Biomechanical modelling and computer aided simulation of deep brain retraction in neurosurgery, Comput. Methods Programs Biomed. 197 (2020) 105688, doi:10.1016/j.cmpb.2020.105688.
[106] M.T. Prange, S.S. Margulies, Regional, directional, and age-dependent properties of the brain undergoing large deformation, J. Biomech. Eng. 124 (2) (2002) 244–252, doi:10.1115/1.1449907.
[107] F. Velardi, F. Fraternali, M. Angelillo, Anisotropic constitutive equations and experimental tensile behavior of brain tissue, Biomech. Model. Mechanobiol. 5 (1) (2006) 53–61, doi:10.1007/s10237-005-0007-9.
[108] B.S. Elkin, A. Ilankova, B. Morrison, Dynamic, regional mechanical properties of the porcine brain: indentation in the coronal plane, J. Biomech. Eng. 133 (7) (2011) 071009., doi:10.1115/1.4004494.
[109] S. Budday, R. Nay, R. de Rooij, P. Steinmann, T. Wyrobek, T.C. Ovaert, E. Kuhl, Mechanical properties of gray and white matter brain tissue by indentation, J. Mech. Behav. Biomed. Mater. 46 (2015) 318–330, doi:10.1016/j.jmbbm.2015.02.024.
[110] S. Budday, G. Sommer, C. Birkl, C. Langkammer, J. Haybaeck, J. Kohnert, M. Bauer, F. Paulsen, P. Steinmann, E. Kuhl, G.A. Holzapfel, Mechanical characterization of human brain tissue, Acta Biomater. 48 (2017) 319–340, doi:10.1016/j.actbio.2016.10.036.
[111] A. Samadi-Dooki, G.Z. Voyiadjis, R.W. Stout, An indirect indentation method for evaluating the linear viscoelastic properties of the brain tissue, J. Biomech. Eng. 139 (6) (2017) ., doi:10.1115/1.4036486.
[112] S.N. Sundaresh, J.D. Finan, B.S. Elkin, A.V. Basilio, G.M. McKhann, B.M. Rd, Region-dependent viscoelastic properties of human brain tissue under large deformations, Ann. Biomed. Eng. 50 (11) (2022) 1452–1460, doi:10.1007/s10439-022-02910-7.
[113] J.A.W. van Dommelen, T.P.J. van der Sande, M. Hrapko, G.W.M. Peters, Mechanical properties of brain tissue by indentation: interregional variation, J. Mech. Behav. Biomed. Mater. 3 (2) (2010) 158–166, doi:10.1016/j.jmbbm.2009.09.001.
[114] J. Weickenmeier, R. de Rooij, S. Budday, T.C. Ovaert, E. Kuhl, The mechanical importance of myelination in the central nervous system, J. Mech. Behav. Biomed. Mater. 76 (2017) 119–124, doi:10.1016/j.jmbbm.2017.04.017.
[115] A. Samadi-Dooki, G.Z. Voyiadjis, R.W. Stout, A combined experimental, modeling, and computational approach to interpret the viscoelastic response of the white matter brain tissue during indentation, J. Mech. Behav. Biomed. Mater. 77 (2018) 24–33, doi:10.1016/j.jmbbm.2017.08.037.
[116] A. Menichetti, D.B. MacManus, M.D. Gilchrist, B. Depreitere, J. Vander Sloten, N. Famaey, Regional characterization of the dynamic mechanical properties of human brain tissue by microindentation, Int. J. Eng. Sci. 155 (2020) 103355, doi:10.1016/j.ijengsci.2020.103355.
[117] L. Qian, H. Zhao, Y. Guo, Y. Li, M. Zhou, L. Yang, Z. Wang, Y. Sun, Influence of strain rate on indentation response of porcine brain, J. Mech. Behav. Biomed. Mater. 82 (2018) 210–217, doi:10.1016/j.jmbbm.2018.03.031.
[118] Z. Du, Z. Li, P. Wang, Z. Zhuang, Z. Liu, Revealing the nonlinear mechanical behavior of white matter brain tissue by analyzing the asynchronous deformation and damage of matrix and axonal fibers, Int. J. Solids Struct. 242 (2022) 111554, doi:10.1016/j.ijsolstr.2022.111554.
[119] M. Kohandel, S. Sivaloganathan, G. Tenti, K. Darvish, Frequency dependence of complex moduli of brain tissue using a fractional Zener model, Phys. Med. Biol. 50 (12) (2005) 2799–2805, doi:10.1088/0031-9155/50/12/005.
[120] G. Davis, M. Kohandel, S. Sivaloganathan, G. Tenti, The constitutive properties of the brain paraenchyma Part 2. Fractional derivative approach, Med. Eng. Phys. 28 (5) (2006) 455–459, doi:10.1016/j.medengphy.2005.07.023.
[121] M. Hrapko, J.A. Van Dommelen, G.W. Peters, J.S. Wismans, The mechanical behaviour of brain tissue: large strain response and constitutive modelling, Biorheology 43 (2006) 59–69. ISBN: 2951421060
[122] T.P. Prevost, A. Balakrishnan, S. Suresh, S. Socrate, Biomechanics of brain tissue, Acta Biomater. 7 (1) (2011) 83–95, doi:10.1016/j.actbio.2010.06.035.
[123] S. Budday, G. Sommer, G.A. Holzapfel, P. Steinmann, E. Kuhl, Viscoelastic parameter identification of human brain tissue, J. Mech. Behav. Biomed. Mater. 74 (2017) 463–476, doi:10.1016/j.jmbbm.2017.07.014.
[124] K. Haldar, C. Pal, Rate dependent anisotropic constitutive modeling of brain tissue undergoing large deformation, J. Mech. Behav. Biomed. Mater. 81 (2018) 178–194, doi:10.1016/j.jmbbm.2017.12.021.
[125] S. Reese, S. Govindjee, A theory of finite viscoelasticity and numerical aspects, Int. J. Solids Struct. 35 (26-27) (1998) 3455–3482, doi:10.1016/S0020-7683(97)00217-5.
[126] Y. Feng, R.J. Okamoto, R. Namani, G.M. Genin, P.V. Bayly, Measurements of mechanical anisotropy in brain tissue and implications for transversely isotropic material models of white matter, J. Mech. Behav. Biomed. Mater. 23 (2013) 117–132, doi:10.1016/j.jmbbm.2013.04.007.
[127] A. Jamal, A. Bernardini, D. Dini, Microscale characterisation of the time-dependent mechanical behaviour of brain white matter, J. Mech. Behav. Biomed. Mater. 125 (2022) 104917, doi:10.1016/j.jmbbm.2021.104917.
[128] R.J.H. Cloots, J.A.W. van Dommelen, T. Nyberg, S. Kleiven, M.G.D. Geers, Micromechanics of diffuse axonal injury: influence of axonal orientation and anisotropy, Biomech. Model. Mechanobiol. 10 (3) (2011) 413–422, doi:10.1007/s10237-010-0243-5.
[129] C. Giordano, S. Kleiven, Connecting fractional anisotropy from medical images with mechanical anisotropy of a hyperviscoelastic fibre-reinforced constitutive model for brain tissue, J. R. Soc. Interface 11 (91) (2014) 20130914, doi:10.1098/rsif.2013.0914.
[130] K.M. Labus, C.M. Puttlitz, An anisotropic hyperelastic constitutive model of brain white matter in biaxial tension and structural-mechanical relationships, J. Mech. Behav. Biomed. Mater. 62 (2016) 195–208, doi:10.1016/j.jmbbm.2016.05.003.
[131] F. Pervin, W.W. Chen, Dynamic mechanical response of bovine gray matter and white matter brain tissues under compression, J. Biomech. 42 (6) (2009) 731–735, doi:10.1016/j.jbiomech.2009.01.023.
[132] S. Saeidi, M.P. Kainz, M. Dalbosco, M. Terzano, G.A. Holzapfel, Histology-informed multiscale modeling of human brain white matter, Sci. Rep. 13 (1) (2023) 19641, doi:10.1038/s41598-023-46600-3.
[133] J. Ciambella, P. Nardinocchi, A structurally frame-indifferent model for anisotropic visco-hyperelastic materials, J. Mech. Phys. Solids 147 (2021) 104247, doi:10.1016/j.jmps.2020.104247.
[134] G.A. Holzapfel, Nonlinear Solid Mechanics: A Continuum Approach for Engineering Science, Wiley, Chichester, 2000.
[135] E. Comellas, S. Budday, J.-P. Pelteret, G.A. Holzapfel, P. Steinmann, Modeling the porous and viscous responses of human brain tissue behavior, Comput. Methods Appl. Mech. Eng. 369 (2020) 113128, doi:10.1016/j.cma.2020.113128.
[136] M. Kaczmarek, The hydromechanics of hydrocephalus: steady-state solutions for cylindrical geometry, Bull. Math. Biol. 59 (2) (1997) 295–323, doi:10.1016/S0092-8240(96)00073-0.

[137] S. Gholampour, N. Fatouraee, Boundary conditions investigation to improve computer simulation of cerebrospinal fluid dynamics in hydrocephalus patients, Commun. Biol. 4 (394) (2021) 1–15, doi:10.1038/s42003-021-01920-w.
[138] S. Gholampour, D. Frim, B. Yamini, Long-term recovery behavior of brain tissue in hydrocephalus patients after shunting, Commun. Biol. 5 (1198) (2022) 1–13, doi:10.1038/s42003-022-04128-8.
[139] R.M. Bowen, Theory of mixtures, in: A.C. Eringen (Ed.), Continuum Physics, 3, Academic Press, New York, 1976.
[140] V.C. Mow, S.C. Kuei, W.M. Lai, C.G. Armstrong, Biphasic creep and stress relaxation of articular cartilage in compression: theory and experiments, J. Biomech. Eng. 102 (1) (1980) 73–84, doi:10.1115/1.3138202.
[141] W. Ehlers, A. Wagner, Multi-component modelling of human brain tissue: a contribution to the constitutive and computational description of deformation, flow and diffusion processes with application to the invasive drug-delivery problem, Comput. Methods Biomech. Biomed. Eng. 5842 (8) (2015) 861–879, doi:10.1080/10255842.2013.853754.
[142] S. Cheng, L.E. Bilston, Unconfined compression of white matter, J. Biomech. 40 (1) (2007) 117–124, doi:10.1016/j.jbiomech.2005.11.004.
[143] A. Greiner, N. Reiter, F. Paulsen, G.A. Holzapfel, P. Steinmann, E. Comellas, S. Budday, Poro-viscoelastic effects during biomechanical testing of human brain tissue, Front. Mech. Eng. 7 (2021), doi:10.3389/fmech.2021.708350.
[144] S. Urcun, P.-Y. Rohan, G. Sciumé, S.P.A. Bordas, Cortex tissue relaxation and slow to medium load rates dependency can be captured by a two-phase flow poroelastic model, J. Mech. Behav. Biomed. Mater. 126 (2022) 104952, doi:10.1016/j.jmbbm.2021.104952.
[145] W. Ehlers, M. Morrison, P. Schröder, D. Stöhr, A. Wagner, Multiphasic modelling and computation of metastatic lung-cancer cell proliferation and atrophy in brain tissue based on experimental data, Biomech. Model. Mechanobiol. 21 (1) (2022) 277–315, doi:10.1007/s10237-021-01535-4.
[146] M.A. Biot, General theory of three-dimensional consolidation, J. Appl. Phys. 12 (2) (1941) 155–164, doi:10.1063/1.1712886.
[147] M.A. Biot, Theory of finite deformations of porous solids, Indiana Univ. Math. J. 21 (7) (1972) 597–620.
[148] S. Sivaloganathan, M. Stastna, G. Tenti, J.M. Drake, Biomechanics of the brain: a theoretical and numerical study of Biot's equations of consolidation theory with deformation-dependent permeability, Int. J. Non-Linear Mech. 40 (9) (2005) 1149–1159, doi:10.1016/j.ijnonlinmec.2005.04.004.
[149] B. Wirth, I. Sobey, An axisymmetric and fully 3D poroelastic model for the evolution of hydrocephalus, Math. Med. Biol. 23 (4) (2006) 363–388, doi:10.1093/imammb/dql014.
[150] I. Sobey, B. Wirth, Effect of non-linear permeability in a spherically symmetric model of hydrocephalus, Math. Med. Biol. 23 (4) (2006) 339–361, doi:10.1093/imammb/dql015.
[151] A. Mehrabian, Y. Abousleiman, General solutions to poroviscoelastic model of hydrocephalic human brain tissue, J. Theor. Biol. 291 (1) (2011) 105–118, doi:10.1016/j.jtbi.2011.09.011.
[152] T. Dutta-Roy, A. Wittek, K. Miller, Biomechanical modelling of normal pressure hydrocephalus, J. Biomech. 41 (10) (2008) 2263–2271, doi:10.1016/j.jbiomech.2008.04.014.
[153] J.J. Garcia, J.H. Smith, A biphasic hyperelastic model for the analysis of fluid and mass transport in brain tissue, Ann. Biomed. Eng. 37 (2) (2009) 375–386, doi:10.1007/s10439-008-9610-0.
[154] J.H. Smith, J.J. Garcia, A nonlinear biphasic model of flow-controlled infusion in brain: fluid transport and tissue deformation analyses, J. Biomech. 42 (13) (2009) 2017–2025, doi:10.1016/j.jbiomech.2009.06.014.
[155] M. Hosseini-Farid, M. Ramzanpour, J. McLean, M. Ziejewski, G. Karami, A poro-hyper-viscoelastic rate-dependent constitutive modeling for the analysis of brain tissues, J. Mech. Behav. Biomed. Mater. 102 (2020) 103475, doi:10.1016/j.jmbbm.2019.103475.
[156] W. Ehlers, G. Eipper, Finite elastic deformations in liquid-saturated and empty porous solids, in: Porous Media: Theory and Experiments, 34, Springer Netherlands, Dordrecht, 1999, pp. 179–191.
[157] G.A. Ateshian, J.A. Weiss, Anisotropic hydraulic permeability under finite deformation, J. Biomech. Eng. 132 (11) (2010) 1–7, doi:10.1115/1.4002588.
[158] K. Miller, K. Chinzei, G. Orssengo, P. Bednarz, Mechanical properties of brain tissue in-vivo: experiment and computer simulation, J. Biomech. 33 (11) (2000) 1369–1376, doi:10.1016/s0021-9290(00)00120-2.
[159] A. Gefen, S.S. Margulies, Are in vivo and in situ brain tissues mechanically similar? J. Biomech. 37 (9) (2004) 1339–1352, doi:10.1016/j.jbiomech.2003.12.032.
[160] S. Mehdizadeh, M. Khoshgoftar, N. Siamak, F. Farhad, A. Hooshiar, Comparison between brain tissue gray and white matters in tension including necking phenomenon, Am. J. Appl. Sci. 5 (2008), doi:10.3844/ajassp.2008.1701.1706.
[161] T.P. Prevost, G. Jin, M.A. de Moya, H.B. Alam, S. Suresh, S. Socrate, Dynamic mechanical response of brain tissue in indentation in vivo, in situ and in vitro, Acta Biomater. 7 (12) (2011) 4090–4101, doi:10.1016/j.actbio.2011.06.032.
[162] T. Kaster, I. Sack, A. Samani, Measurement of the hyperelastic properties of ex vivo brain tissue slices, J. Biomech. 44 (6) (2011) 1158–1163, doi:10.1016/j.jbiomech.2011.01.019.
[163] B. Rashid, M. Destrade, M.D. Gilchrist, Mechanical characterization of brain tissue in compression at dynamic strain rates, J. Mech. Behav. Biomed. Mater. 10 (2012) 23–38, doi:10.1016/j.jmbbm.2012.01.022.
[164] B. Rashid, M. Destrade, M.D. Gilchrist, Mechanical characterization of brain tissue in tension at dynamic strain rates, J. Mech. Behav. Biomed. Mater. 33 (2014) 43–54, doi:10.1016/j.jmbbm.2012.07.015.
[165] Z. Zhu, C. Jiang, H. Jiang, A visco-hyperelastic model of brain tissue incorporating both tension/compression asymmetry and volume compressibility, Acta Mech. 230 (6) (2019) 2125–2135, doi:10.1007/s00707-019-02383-1.
[166] F. Eskandari, M. Shafieian, M.M. Aghdam, K. Laksari, Tension strain-softening and compression strain-stiffening behavior of brain white matter, Ann. Biomed. Eng. 49 (1) (2021) 276–286, doi:10.1007/s10439-020-02541-w.
[167] G.M. Boiczyk, N. Pearson, V.B. Kote, A. Sundaramurthy, D.R. Subramaniam, J.E. Rubio, G. Unnikrishnan, J. Reifman, K.L. Monson, Rate- and region-dependent mechanical properties of Göttingen minipig brain tissue in simple shear and unconfined compression, J. Biomech. Eng. 145 (6) (2023) 061004., doi:10.1115/1.4056480.
[168] N. Abolhassani, R. Patel, M. Moallem, Needle insertion into soft tissue: a survey, Med. Eng. Phys. 29 (4) (2007) 413–431, doi:10.1016/j.medengphy.2006.07.003.
[169] B. Takabi, B.L. Tai, A review of cutting mechanics and modeling techniques for biological materials, Med. Eng. Phys. 45 (2017) 1–14, doi:10.1016/j.medengphy.2017.04.004.
[170] F. Zhong, Y. Wang, Z. Wang, Y.-H. Liu, Dual-arm robotic needle insertion with active tissue deformation for autonomous suturing, IEEE Rob. Autom. Lett. 4 (3) (2019) 2669–2676, doi:10.1109/LRA.2019.2913082.
[171] W. Wu, C. Xu, C. Pan, Z. Huang, J. Zhou, P. Huang, Effect of vibration frequency on frictional resistance of brain tissue during vibration-assisted needle insertion, Med. Eng. Phys. 86 (2020) 35–40, doi:10.1016/j.medengphy.2020.10.003.
[172] Y. Tang, J. Zou, R.C.C. Flesch, T. Jin, Backflow modeling in nanofluid infusion and analysis of its effects on heat induced damage during magnetic hyperthermia, Appl. Math. Model. 114 (2023) 583–600, doi:10.1016/j.apm.2022.10.020.
[173] F. Casanova, P.R. Carney, M. Sarntinoranont, In vivo evaluation of needle force and friction stress during insertion at varying insertion speed into the brain, J. Neurosci. Methods 237 (2014) 79–89, doi:10.1016/j.jneumeth.2014.08.012.
[174] C. Simone, A.M. Okamura, Modeling of needle insertion forces for robot-assisted percutaneous therapy, in: Proceedings 2002 IEEE International Conference on Robotics and Automation, 2, 2002, pp. 2085–2091, doi:10.1109/ROBOT.2002.1014848.
[175] S. DiMaio, S. Salcudean, Needle insertion modeling and simulation, IEEE Trans. Rob. Autom. 19 (5) (2003) 864–875, doi:10.1109/TRA.2003.817044.
[176] A.M. Okamura, C. Simone, M. O'Leary, Force modeling for needle insertion into soft tissue, IEEE Trans. Biomed. Eng. 51 (10) (2004) 1707–1716, doi:10.1109/TBME.2004.831542.
[177] S. DiMaio, S. Salcudean, Needle steering and motion planning in soft tissues, IEEE Trans. Biomed. Eng. 52 (6) (2005) 965–974, doi:10.1109/TBME.2005.846734.
[178] A. Wittek, T. Dutta-Roy, Z. Taylor, A. Horton, T. Washio, K. Chinzei, K. Miller, Subject-specific non-linear biomechanical model of needle insertion into brain, Comput. Methods Biomech. Biomed. Eng. 11 (2) (2008) 135–146, doi:10.1080/10255840701688095.
[179] X. Chen, M. Sarntinoranont, Biphasic finite element model of solute transport for direct infusion into nervous tissue, Ann. Biomed. Eng. 35 (12) (2007) 2145–2158, doi:10.1007/s10439-007-9371-1.
[180] J.J. García, J.H. Smith, A biphasic hyperelastic model for the analysis of fluid and mass transport in brain tissue, Ann. Biomed. Eng. 37 (2) (2009) 375–386, doi:10.1007/s10439-008-9610-0.
[181] O.A. Shergold, N.A. Fleck, Mechanisms of deep penetration of soft solids, with application to the injection and wounding of skin, Proc. R. Soc. A Math. Phys. Eng. Sci. 460 (2050) (2004) 3037–3058, doi:10.1098/rspa.2004.1315.
[182] T. Azar, V. Hayward, Estimation of the fracture toughness of soft tissue from needle insertion, in: F. Bello, P.J.E. Edwards (Eds.), Biomedical Simulation, Springer Berlin Heidelberg, Berlin, Heidelberg, 2008, pp. 166–175.
[183] M. Khadem, C. Rossa, R.S. Sloboda, N. Usmani, M. Tavakoli, Mechanics of tissue cutting during needle insertion in biological tissue, IEEE Rob. Autom. Lett. 1 (2) (2016) 800–807, doi:10.1109/LRA.2016.2528301.
[184] M. Kuna, Finite Elements in Fracture Mechanics: Theory - Numerics - Applications, Springer Netherlands, Heidelberg, 2013.
[185] M. Terzano, A. Spagnoli, P. Ståhle, A fracture mechanics model to study indentation cutting, Fatigue Fract. Eng. Mater. Struct. 41 (4) (2018) 821–830, doi:10.1111/ffe.12750.
[186] H. Mohammadi, A. Ebrahimian, N. Maftoon, Finite-element modelling of needle-tissue interactions, Arch. Comput. Methods Eng. (2023), doi:10.1007/s11831-023-10020-3. https://link.springer.com/10.1007/s11831-023-10020-3
[187] S. Misra, K.B. Reed, A.S. Douglas, K.T. Ramesh, A.M. Okamura, Needle-tissue interaction forces for bevel-tip steerable needles, in: 2008 2nd IEEE RAS & EMBS International Conference on Biomedical Robotics and Biomechatronics, 2008, pp. 224–231, doi:10.1109/BIOROB.2008.4762872. ArXiv: NIHMS150003 ISSN: 2155-1774
[188] M. Mahvash, P. Dupont, Mechanics of dynamic needle insertion into a biological material, IEEE Trans. Biomed. Eng. 57 (4) (2010) 934–943, doi:10.1109/TBME.2009.2036856.
[189] M. Oldfield, D. Dini, G. Giordano, F. Rodriguez y. Baena, Detailed finite element modelling of deep needle insertions into a soft tissue phantom using a cohesive approach, Comput. Methods Biomech. Biomed. Eng. 16 (5) (2013) 530–543, doi:10.1080/10255842.2011.628448.
[190] J.D. Toaquiza Tubon, O. Moreno-Flores, V.D. Sree, A.B. Tepole, Anisotropic damage model for collagenous tissues and its application to model fracture and needle insertion mechanics, Biomech. Model. Mechanobiol. 21 (6) (2022) 1–16, doi:10.1007/s10237-022-01624-y. Publisher: Springer Berlin Heidelberg ISBN: 0123456789

[191] A. Wittek, G. Bourantas, B.F. Zwick, G. Joldes, L. Esteban, K. Miller, Mathematical modeling and computer simulation of needle insertion into soft tissue, PLOS ONE 15 (12) (2020) e0242704, doi:10.1371/journal.pone.0242704.
[192] A.A. Yakovenko, Y.-X. Lai, I.G. Goryacheva, M.-S. Ju, M.Z. Dosaev, Y.D. Selyutskiy, Modeling and experimental study of the needle indentation into a brain phantom, Int. J. Non-Linear Mech. 137 (2021) 103832, doi:10.1016/j.ijnonlinmec.2021.103832.
[193] E. Lueshen, K. Tangen, A.I. Mehta, A. Linninger, Backflow-free catheters for efficient and safe convection-enhanced delivery of therapeutics, Med. Eng. Phys. 45 (2017) 15–24, doi:10.1016/j.medengphy.2017.02.018.
[194] G.A. Orozco, J.H. Smith, J.J. García, Three-dimensional nonlinear finite element model to estimate backflow during flow-controlled infusions into the brain, Proc. Inst. Mech. Eng. H 234 (9) (2020) 1018–1028, doi:10.1177/0954411920937220.
[195] J.J. García, A.B. Molano, J.H. Smith, Description and validation of a finite element model of backflow during infusion into a brain tissue phantom, J. Comput. Nonlinear Dyn. 8 (1) (2013), doi:10.1115/1.4007311.
[196] O. Ivanchenko, N. Sindhwani, A. Linninger, Experimental techniques for studying poroelasticity in brain phantom gels under high flow microinfusion, J. Biomech. Eng. 132 (5) (2010), doi:10.1115/1.4001164.
[197] E. Axpe, G. Orive, K. Franze, E.A. Appel, Towards brain-tissue-like biomaterials, Nat. Commun. 11 (3423) (2020) 1–4, doi:10.1038/s41467-020-17245-x.
[198] X. Chen, G.W. Astary, H. Sepulveda, T.H. Mareci, M. Sarntinoranont, Quantitative assessment of macromolecular concentration during direct infusion into an agarose hydrogel phantom using contrast-enhanced MRI, Magn. Reson. Imaging 26 (10) (2008) 1433–1441, doi:10.1016/j.mri.2008.04.011.
[199] P. Nakielski, T. Kowalczyk, K. Zembrzycki, T.A. Kowalewski, Experimental and numerical evaluation of drug release from nanofiber mats to brain tissue, J. Biomed. Mater. Res. Part B 103 (2) (2015) 282–291, doi:10.1002/jbm.b.33197.
[200] Z. Tan, J.P. Ewen, A.E. Forte, S. Galvan, E. De Momi, F. Rodriguez y. Baena, D. Dini, What does a brain feel like? J. Chem. Educ. 97 (11) (2020) 4078–4083, doi:10.1021/acs.jchemed.0c00957.
[201] A.E. Forte, S. Galvan, F. Manieri, F. Rodriguez y. Baena, D. Dini, A composite hydrogel for brain tissue phantoms, Mater. Des. 112 (2016) 227–238, doi:10.1016/j.matdes.2016.09.063.
[202] A.E. Forte, S. Galvan, D. Dini, Models and tissue mimics for brain shift simulations, Biomech. Model. Mechanobiol. 17 (1) (2018) 249–261, doi:10.1007/s10237-017-0958-7.
[203] Z. Tan, D. Dini, F. Rodriguez y. Baena, A.E. Forte, Composite hydrogel: a high fidelity soft tissue mimic for surgery, Mater. Des. 160 (2018) 886–894, doi:10.1016/j.matdes.2018.10.018.
[204] M.P. Kainz, A. Greiner, J. Hinrichsen, D. Kolb, E. Comellas, P. Steinmann, S. Budday, M. Terzano, G.A. Holzapfel, Poro-viscoelastic material parameter identification of brain tissue-mimicking hydrogels, Front. Bioeng. Biotechnol. 11 (2023), doi:10.3389/fbioe.2023.1143304.
[205] A.I. Lavrova, A.V. Sychev, A.S. Vanina, E.V. Grekhnyova, E.B. Postnikov, Accessing random diffusivity in a hydrogel-based brain's paranchyma phantom, in: 2022 7th International Conference on Intelligent Informatics and Biomedical Science (ICIIBMS), IEEE, 2022, pp. 24–26, doi:10.1109/ICIIBMS55689.2022.9971620.
[206] T. Distler, E. Schaller, P. Steinmann, A.R. Boccaccini, S. Budday, Alginate-based hydrogels show the same complex mechanical behavior as brain tissue, J. Mech. Behav. Biomed. Mater. 111 (2020) 103979, doi:10.1016/j.jmbbm.2020.103979.
[207] A.S. Vanina, A.V. Sychev, A.I. Lavrova, P.V. Gavrilov, P.L. Andropova, E.V. Grekhnyova, T.N. Kudryavtseva, E.B. Postnikov, A hydrogel-based phantom of the brain tissue aimed at modelling complex metabolic transport processes, Eur. Phys. J. Spec. Top. (2022) 1–9, doi:10.1140/epjs/s11734-022-00733-0.
[208] A. Leibinger, A.E. Forte, Z. Tan, M.J. Oldfield, F. Beyrau, D. Dini, F. Rodriguez y. Baena, Soft tissue phantoms for realistic needle insertion: a comparative study, Ann. Biomed. Eng. 44 (8) (2016) 2442–2452, doi:10.1007/s10439-015-1523-0.
[209] A.E. Forte, F. D'Amico, M.N. Charalambides, D. Dini, J.G. Williams, Modelling and experimental characterisation of the rate dependent fracture properties of gelatine gels, Food Hydrocolloids 46 (2015) 180–190, doi:10.1016/j.foodhyd.2014.12.028.
[210] M. Navarro-Lozoya, M.S. Kennedy, D. Dean, J.I. Rodriguez-Devora, Development of phantom material that resembles compression properties of human brain tissue for training models, Materialia 8 (2019) 100438, doi:10.1016/j.mtla.2019.100438.
[211] A. Tejo-Otero, F. Fenollosa-Artés, I. Achaerandio, S. Rey-Vinolas, I. Buj-Corral, M.Á. Mateos-Timoneda, E. Engel, Soft-tissue-mimicking using hydrogels for the development of phantoms, Gels 8 (1) (2022) 40., doi:10.3390/gels8010040.
[212] S.D. Kim, K. Kim, M. Shin, Recent advances in 3D printable conductive hydrogel inks for neural engineering, Nano Convergence 10 (1) (2023) 1–19, doi:10.1186/s40580-023-00389-z.
[213] F. Dell'Isola, D. Steigmann, A.D. Corte, Synthesis of fibrous complex structures: designing microstructure to deliver targeted macroscale response, Appl. Mech. Rev. 67 (6) (2015), doi:10.1115/1.4032206.
[214] N. Rott, Note on the history of the Reynolds number, Annu. Rev. Fluid Mech. 22 (1) (1990) 1–12, doi:10.1146/annurev.fl.22.010190.000245.
[215] X. Kong, Y. Yang, J. Gan, T. Yuan, L. Ao, W. Wu, Experimental and numerical investigation on the detailed buckling process of similar stiffened panels subjected to in-plane compressive load, Thin-Walled Struct. 148 (2020) 106620, doi:10.1016/j.tws.2020.106620.
[216] T. Yuan, Y. Yang, X. Kong, W. Wu, Similarity criteria for the buckling process of stiffened plates subjected to compressive load, Thin-Walled Struct. 158 (2021) 107183, doi:10.1016/j.tws.2020.107183.
[217] Z. Wang, T. Yuan, X. Kong, W. Wu, A universal similarity method and design procedure for buckling assessment of stiffened plates under compression load on real ships, Thin-Walled Struct. 181 (2022) 110025, doi:10.1016/j.tws.2022.110025.
[218] J. Bakarji, J. Callaham, S.L. Brunton, J.N. Kutz, Dimensionally consistent learning with Buckingham Pi, Nat. Comput. Sci. 2 (2022) 834–844, doi:10.1038/s43588-022-00355-5.
[219] X. Xie, A. Samaei, J. Guo, W.K. Liu, Z. Gan, Data-driven discovery of dimensionless numbers and governing laws from scarce measurements, Nat. Commun. 13 (7562) (2022) 1–11, doi:10.1038/s41467-022-35084-w.
[220] E.P. Chan, Y. Hu, P.M. Johnson, Z. Suo, C.M. Stafford, Spherical indentation testing of poroelastic relaxations in thin hydrogel layers, Soft Matter 8 (5) (2012) 1492–1498, doi:10.1039/C1SM06514A.
[221] M. Wang, S. Liu, Z. Xu, K. Qu, M. Li, X. Chen, Q. Xue, G.M. Genin, T.J. Lu, F. Xu, Characterizing poroelasticity of biological tissues by spherical indentation: an improved theory for large relaxation, J. Mech. Phys. Solids 138 (2020), doi:10.1016/j.jmps.2020.103920.
[222] S. Chatelin, A. Constantinesco, R. Willinger, Fifty years of brain tissue mechanical testing: from in vitro to in vivo investigations, Biorheology 47 (5-6) (2010) 255–276, doi:10.3233/BIR-2010-0576.
[223] M.C. Murphy, J. Huston, R.L. Ehman, MR elastography of the brain and its application in neurological diseases, Neuroimage 187 (2019) 176–183, doi:10.1016/j.neuroimage.2017.10.008.
[224] H. Herthum, S.C.H. Dempsey, A. Samani, F. Schrank, M. Shahryari, C. Warmuth, H. Tzschätzsch, J. Braun, I. Sack, Superviscous properties of the in vivo brain at large scales, Acta Biomater. 121 (2021) 393–404, doi:10.1016/j.actbio.2020.12.027.
[225] L.V. Hiscox, C.L. Johnson, M.D.J. McGarry, M. Perrins, A. Littlejohn, E.J.R. van Beek, N. Roberts, J.M. Starr, High-resolution magnetic resonance elastography reveals differences in subcortical gray matter viscoelasticity between young and healthy older adults, Neurobiol. Aging 65 (2018) 158, doi:10.1016/j.neurobiolaging.2018.01.010.
[226] A. Arani, A. Manduca, R.L. Ehman, J.H. Iii, Harnessing brain waves: a review of brain magnetic resonance elastography for clinicians and scientists entering the field, Br. J. Radiol. (2021). https://www.birpublications.org/doi/10.1259/bjr.20200265
[227] E. Spedden, J.D. White, E.N. Naumova, D.L. Kaplan, C. Staii, Elasticity maps of living neurons measured by combined fluorescence and atomic force microscopy, Biophys. J. 103 (5) (2012) 868–877, doi:10.1016/j.bpj.2012.08.005.
[228] K.B. Bernick, T.P. Prevost, S. Suresh, S. Socrate, Biomechanics of single cortical neurons, Acta Biomater. 7 (3) (2011) 1210–1219, doi:10.1016/j.actbio.2010.10.018.
[229] Y.-B. Lu, K. Franze, G. Seifert, C. Steinhäuser, F. Kirchhoff, H. Wolburg, J. Guck, P. Janmey, E.-Q. Wei, J. Käs, A. Reichenbach, Viscoelastic properties of individual glial cells and neurons in the CNS, Proc. Natl. Acad. Sci. U.S.A. 103 (47) (2006) 17759–17764, doi:10.1073/pnas.0606150103.
[230] F. Hasan, K. Al Mahmud, Md.I. Khan, A. Adnan, Front. Bioeng. Biotechnol. 10 (2022), doi:10.3389/fbioe.2022.904818.
[231] Y. Zhang, K. Abiraman, H. Li, D.M. Pierce, A.V. Tzingounis, G. Lykotrafitis, Modeling of the axon membrane skeleton structure and implications for its mechanical properties, PLoS Comput. Biol. 13 (2) (2017) e1005407, doi:10.1371/journal.pcbi.1005407.
[232] M. Dao, C.T. Lim, S. Suresh, Mechanics of the human red blood cell deformed by optical tweezers, J. Mech. Phys. Solids 51 (11) (2003) 2259–2280, doi:10.1016/j.jmps.2003.09.019.
[233] J. Sigüenza, S. Mendez, F. Nicoud, How should the optical tweezers experiment be used to characterize the red blood cell membrane mechanics? Biomech. Model. Mechanobiol. 16 (5) (2017) 1645–1657, doi:10.1007/s10237-017-0910-x.
[234] E.P.S. Tan, S.Y. Ng, C.T. Lim, Tensile testing of a single ultrafine polymeric fiber, Biomaterials 26 (13) (2005) 1453–1456, doi:10.1016/j.biomaterials.2004.05.021.
[235] X. Tang, X. Liu, P. Li, D. Liu, M. Kojima, Q. Huang, T. Arai, Efficient single-cell mechanical measurement by integrating a cell arraying microfluidic device with magnetic tweezer, IEEE Rob. Autom. Lett. 6 (2) (2021) 2978–2984, doi:10.1109/LRA.2021.3062793.
[236] K.C. Neuman, A. Nagy, Single-molecule force spectroscopy: optical tweezers, magnetic tweezers and atomic force microscopy, Nat. Methods 5 (6) (2008) 491–505, doi:10.1038/nmeth.1218.
[237] E. Spedden, C. Staii, Neuron biomechanics probed by atomic force microscopy, Int. J. Mol. Sci. 14 (8) (2013) 16124–16140, doi:10.3390/ijms140816124.
[238] Y. Wu, C. Whiteus, C.S. Xu, K.J. Hayworth, R.J. Weinberg, H.F. Hess, P. De Camilli, Contacts between the endoplasmic reticulum and other membranes in neurons, Proc. Natl. Acad. Sci. U.S.A. 114 (24) (2017) E4859–E4867, doi:10.1073/pnas.1701078114.
[239] A. Bernardini, M. Trovatelli, M.M. Kłosowski, M. Pederzani, D.D. Zani, S. Brizzola, A. Porter, F. Rodriguez y. Baena, D. Dini, Reconstruction of ovine axonal cytoarchitecture enables more accurate models of brain biomechanics, Commun. Biol. 5 (1101) (2022) 1–14, doi:10.1038/s42003-022-04052-x.

[240] M. Sarntinoranont, R.K. Banerjee, R.R. Lonser, P.F. Morrison, A computational model of direct interstitial infusion of macromolecules into the spinal cord, Ann. Biomed. Eng. 31 (4) (2003) 448.
[241] J.H. Kim, G.W. Astary, X. Chen, T.H. Mareci, M. Sarntinoranont, Voxelized model of interstitial transport in the rat spinal cord following direct infusion into white matter, J. Biomech. Eng. 131 (7) (2009), doi:10.1115/1.3169248.
[242] J.H. Kim, T.H. Mareci, M. Sarntinoranont, A voxelized model of direct infusion into the corpus callosum and hippocampus of the rat brain: model development and parameter analysis, Med. Biol. Eng. Comput. 48 (3) (2010) 203–214, doi:10.1007/s11517-009-0564-7.
[243] C.A. Stine, J.M. Munson, Convection-enhanced delivery: connection to and impact of interstitial fluid flow, Front. Oncol. 9 (2019), doi:10.3389/fonc.2019.00966.
[244] A.A. Linninger, C. Tsakiris, D.C. Zhu, M. Xenos, P. Roycewicz, Z. Danziger, R. Penn, Pulsatile cerebrospinal fluid dynamics in the human brain, IEEE Trans. Biomed. Eng. 52 (4) (2005) 557–565, doi:10.1109/TBME.2005.844021.
[245] A.A. Linninger, M. Xenos, D.C. Zhu, M.R. Somayaji, S. Kondapalli, R.D. Penn, Cerebrospinal fluid flow in the normal and hydrocephalic human brain, IEEE Trans. Biomed. Eng. 54 (2) (2007) 291–302, doi:10.1109/TBME.2006.886853.
[246] J.H. Smith, K.A. Starkweather, J.J. García, Implications of transvascular fluid exchange in nonlinear, biphasic analyses of flow-controlled infusion in brain, Bull. Math. Biol. 74 (4) (2012) 881–907, doi:10.1007/s11538-011-9696-7.
[247] A. Wagner, W. Ehlers, Continuum-mechanical analysis of human brain tissue, Proc. Appl. Math. Mech. 10 (1) (2010) 99–100, doi:10.1002/pamm.201010042.
[248] A. Wagner, W. Ehlers, Computational modelling of drug infusion into the anisotropic white-matter tracts of the human brain, Proc. Appl. Math. Mech. 11 (1) (2011) 133–134, doi:10.1002/pamm.201110058.
[249] K.N. Magdoom, G.L. Pishko, L. Rice, C. Pampo, D.W. Siemann, M. Sarntinoranont, MRI-based computational model of heterogeneous tracer transport following local infusion into a mouse hind limb tumor, PLoS One 9 (3) (2014) e89594, doi:10.1371/journal.pone.0089594.
[250] W. Zhan, D.Y. Arifin, T.K.Y. Lee, C.-H. Wang, Mathematical modelling of convection enhanced delivery of carmustine and paclitaxel for brain tumour therapy, Pharm. Res. 34 (4) (2017) 860–873, doi:10.1007/s11095-017-2114-6.
[251] S.A. Peters, Identification of intestinal loss of a drug through physiologically based pharmacokinetic simulation of plasma concentration-time profiles, Clin. Pharmacokinet. 47 (4) (2008) 245–259, doi:10.2165/00003088-200847040-00003.
[252] W.-C. Chou, Y.-H. Cheng, J.E. Riviere, N.A. Monteiro-Riviere, W.G. Kreyling, Z. Lin, Development of a multi-route physiologically based pharmacokinetic (PBPK) model for nanomaterials: a comparison between a traditional versus a new route-specific approach using gold nanoparticles in rats, Part. Fibre Toxicol. 19 (1) (2022) 1–19, doi:10.1186/s12989-022-00489-4.
[253] D. Deepika, V. Kumar, The role of "Physiologically Based Pharmacokinetic Model (PBPK)" New Approach Methodology (NAM) in pharmaceuticals and environmental chemical risk assessment, Int. J. Environ. Res. Public Health 20 (4) (2023) 3473, doi:10.3390/ijerph20043473.
[254] M. Hammarlund-Udenaes, M. Fridén, S. Syvänen, A. Gupta, On the rate and extent of drug delivery to the brain, Pharm. Res. 25 (8) (2008) 1737–1750, doi:10.1007/s11095-007-9502-2.
[255] J. Westerhout, B. Ploeger, J. Smeets, M. Danhof, E.C.M. de Lange, Physiologically based pharmacokinetic modeling to investigate regional brain distribution kinetics in rats, AAPS J. 14 (3) (2012) 543–553, doi:10.1208/s12248-012-9366-1.
[256] I. Loryan, E. Melander, M. Svensson, M. Payan, F. König, B. Jansson, M. Hammarlund-Udenaes, In-depth neuropharmacokinetic analysis of antipsychotics based on a novel approach to estimate unbound target-site concentration in CNS regions: link to spatial receptor occupancy, Mol. Psychiatry 21 (2016) 1527–1536, doi:10.1038/mp.2015.229.
[257] Y. Yamamoto, P.A. Välitalo, D.R. Huntjens, J.H. Proost, A. Vermeulen, W. Krauwinkel, M.W. Beukers, D.-J. van den Berg, R. Hartman, Y.C. Wong, M. Danhof, J.G.C. van Hasselt, E.C.M. de Lange, Predicting drug concentration-time profiles in multiple CNS compartments using a comprehensive physiologically-based pharmacokinetic model, CPT Pharmacometrics Syst. Pharmacol. 6 (11) (2017) 765–777, doi:10.1002/psp4.12250.
[258] Y. Yamamoto, P.A. Välitalo, Y.C. Wong, D.R. Huntjens, J.H. Proost, A. Vermeulen, W. Krauwinkel, M.W. Beukers, H. Kokki, M. Kokki, M. Danhof, J.G.C. van Hasselt, E.C.M. de Lange, Prediction of human CNS pharmacokinetics using a physiologically-based pharmacokinetic modeling approach, Eur. J. Pharm. Sci. 112 (2018) 168–179, doi:10.1016/j.ejps.2017.11.011.
[259] A.M. Heitman, R.R. Bies, S.L. Schwartz, A physiologically-based pharmacokinetic model of the brain considering regional lipid variance, J. Pharmacol. Exp. Ther. 383 (3) (2022) 217–226, doi:10.1124/jpet.122.001256.
[260] M. Hammarlund-Udenaes, Pharmacokinetic concepts in brain drug delivery, in: Drug Delivery to the Brain, Springer, Cham, Switzerland, 2022, pp. 173–209, doi:10.1007/978-3-030-88773-5_7.
[261] I. Loryan, M. Hammarlund-Udenaes, S. Syvänen, Brain distribution of drugs: pharmacokinetic considerations, Handb. Exp. Pharmacol. 273 (121-150) (2022), doi:10.1007/164_2020_405.
[262] Z.-J. Chen, W.C. Broaddus, R.R. Viswanathan, R. Raghavan, G.T. Gillies, Intraparenchymal drug delivery via positive-pressure infusion: experimental and modeling studies of poroelasticity in brain phantom gels, IEEE Trans. Biomed. Eng. 49 (2) (2002) 85–96, doi:10.1109/10.979348.
[263] J.H. Smith, J.J. Garcíaa, A nonlinear biphasic model of flow-controlled infusion in brain: fluid transport and tissue deformation analyses, J. Biomech. 42 (13) (2009) 2017–2025, doi:10.1016/j.jbiomech.2009.06.014.
[264] J.H. Smith, J. Jaime Garcíaa, A nonlinear biphasic model of flow-controlled infusions in brain: mass transport analyses, J. Biomech. 44 (3) (2011) 524–531, doi:10.1016/j.jbiomech.2010.09.010.
[265] K.H. Støverud, M. Darcis, R. Helmig, S.M. Hassanizadeh, Modeling concentration distribution and deformation during convection-enhanced drug delivery into brain tissue, Transp. Porous Media 92 (1) (2012) 119–143, doi:10.1007/s11242-011-9894-7.
[266] D. Su, R. Ma, L. Zhu, Numerical study of nanofluid infusion in deformable tissues for hyperthermia cancer treatments, Med. Biol. Eng. Comput. 49 (11) (2011) 1233–1240, doi:10.1007/s11517-011-0819-y.
[267] M. Nilsson, J. Lätt, F. Ståhlberg, D. van Westen, H. Hagslätt, The importance of axonal undulation in diffusion MR measurements: a Monte Carlo simulation study, NMR Biomed. 25 (5) (2012) 795–805, doi:10.1002/nbm.1795.
[268] C. Nicholson, P. Kamali-Zare, Reduction of dimensionality in Monte Carlo simulation of diffusion in extracellular space surrounding cubic cells, Neurochem. Res. 45 (1) (2020) 42–52, doi:10.1007/s11064-019-02793-6.
[269] M. Hajiaghamemar, T. Wu, M.B. Panzer, S.S. Margulies, Embedded axonal fiber tracts improve finite element model predictions of traumatic brain injury, Biomech. Model. Mechanobiol. 19 (3) (2020) 1109–1130, doi:10.1007/s10237-019-01273-8.
[270] M. Sarntinoranont, R.K. Banerjee, R.R. Lonser, P.F. Morrison, A computational model of direct interstitial infusion of macromolecules into the spinal cord, Ann. Biomed. Eng. 31 (4) (2003) 448–461, doi:10.1114/1.1558032.
[271] B. Sweetman, M. Xenos, L. Zitella, A.A. Linninger, Three-dimensional computational prediction of cerebrospinal fluid flow in the human brain, Comput. Biol. Med. 41 (2) (2011) 67–75, doi:10.1016/j.compbiomed.2010.12.001.
[272] E. Messaritaki, S.U. Rudrapatna, G.D. Parker, W.P. Gray, D.K. Jones, Improving the predictions of computational models of convection-enhanced drug delivery by accounting for diffusion non-gaussianity, Front. Neurol. 9 (2018), doi:10.3389/fneur.2018.01092.
[273] M. Brady, R. Raghavan, J. Sampson, Determinants of intraparenchymal infusion distributions: modeling and analyses of human glioblastoma trials, Pharmaceutics 12 (9) (2020) 895, doi:10.3390/pharmaceutics12090895.
[274] H. Zhang, T. Schneider, C.A. Wheeler-Kingshott, D.C. Alexander, NODDI: practical in vivo neurite orientation dispersion and density imaging of the human brain, Neuroimage 61 (4) (2012) 1000–1016, doi:10.1016/j.neuroimage.2012.03.072.
[275] A. Jahangiri, A.T. Chin, P.M. Flanigan, R. Chen, K. Bankiewicz, M.K. Aghi, Convection-enhanced delivery in glioblastoma: a review of preclinical and clinical studies, J. Neurosurg. 126 (1) (2017) 191–200, doi:10.3171/2016.1.JNS151591.
[276] D.P.M. Tromp, N. Adluru, A.L. Alexander, M.E. Emborg, Simulating convection-enhanced delivery in the putamen using probabilistic tractography, 2011 IEEE International Symposium on Biomedical Imaging: From Nano to Macro, IEEE, 2011, doi:10.1109/ISBI.2011.5872523. 2011–02
[277] F. Gimenez, M.T. Krauze, F. Valles, P. Hadaczek, J. Bringas, N. Sharma, J. Forsayeth, K.S. Bankiewicz, Image-guided convection-enhanced delivery of GDNF protein into monkey putamen, Neuroimage 54 (2011) S189–S195, doi:10.1016/j.neuroimage.2010.01.023.
[278] M. Brady, R. Raghavan, Z.-J. Chen, W.C. Broaddus, Quantifying fluid infusions and tissue expansion in brain, IEEE Trans. Biomed. Eng. 58 (8) (2011) 2228–2237, doi:10.1109/TBME.2011.2128869.
[279] K.H. Rosenbluth, A.J. Martin, J. Bringas, K.S. Bankiewicz, Evaluation of pressure-driven brain infusions in nonhuman primates by intra-operative 7 tesla MRI, J. Magn. Reson. Imaging 36 (6) (2012) 1339–1346, doi:10.1002/jmri.23771.
[280] I.M.J. van der Bom, R.P. Moser, G. Gao, M. Sena-Esteves, N. Aronin, M.J. Gounis, Frameless multimodal image guidance of localized convection-enhanced delivery of therapeutics in the brain, J. NeuroIntervent. Surg. 5 (1) (2013) 69–72, doi:10.1136/neurintsurg-2011-010170.
[281] R.S. D'Amico, J.A. Neira, J. Yun, N.G. Alexiades, M. Banu, Z.K. Englander, B.C. Kennedy, T.H. Ung, R.J. Rothrock, A. Romanov, X. Guo, B. Zhao, A.M. Sonabend, P. Canoll, J.N. Bruce, Validation of an effective implantable pump-infusion system for chronic convection-enhanced delivery of intracerebral topotecan in a large animal model, J. Neurosurg. 133 (3) (2019) 614–623, doi:10.3171/2019.3.JNS1963.
[282] B. Partridge, A. Eardley, B.E. Morales, S.N. Campelo, M.F. Lorenzo, J.N. Mehta, Y. Kani, J.K.G. Mora, E.-O.Y. Campbell, C.B. Arena, S. Platt, A. Mintz, R.L. Shinn, C.G. Rylander, W. Debinski, R.V. Davalos, J.H. Rossmeisl, Advancements in drug delivery methods for the treatment of brain disease, Front. Vet. Sci. 9 (2022) 1039745, doi:10.3389/fvets.2022.1039745.
[283] S.K. Niazi, Non-invasive drug delivery across the blood–brain barrier: a prospective analysis, Pharmaceutics 15 (11) (2023) 2599, doi:10.3390/pharmaceutics15112599.
[284] D.Y. Arifin, K.Y.T. Lee, C.-H. Wang, Chemotherapeutic drug transport to brain tumor, J. Controlled Release 137 (3) (2009) 203–210, doi:10.1016/j.jconrel.2009.04.013.
[285] L. Vargová, A. Homola, J. Zámečnik, M. Tichý, V. Beneš, E. Syková, Diffusion parameters of the extracellular space in human gliomas, Glia 42 (1) (2003) 77–88, doi:10.1002/glia.10204.
[286] J. Zamecnik, The extracellular space and matrix of gliomas, Acta Neuropathol. 110 (5) (2005) 435–442, doi:10.1007/s00401-005-1078-5.
[287] B.D. Trapp, J. Peterson, R.M. Ransohoff, R. Rudick, S. Mörk, L. Bö, Axonal transection in the lesions of multiple sclerosis, N. Engl. J. Med. (1998), doi:10.1056/NEJM199801293380502.

[288] A. Wilkins, Y. Kondo, J. Song, S. Liu, A. Compston, J.A. Black, S.G. Waxman, I.D. Duncan, Slowly progressive axonal degeneration in a rat model of chronic, nonimmune-mediated demyelination, J. Neuropathol. Exp. Neurol. 69 (12) (2010) 1256–1269, doi:10.1097/NEN.0b013e3181ffc317.
[289] E.K. Nduom, C. Yang, M.J. Merrill, Z. Zhuang, R.R. Lonser, Characterization of the blood-brain barrier of metastatic and primary malignant neoplasms: laboratory investigation, J. Neurosurg. 119 (2) (2013) 427–433, doi:10.3171/2013.3.JNS122226.
[290] A. Bhandari, B. Gu, F.M. Kashkooli, W. Zhan, Image-based predictive modelling frameworks for personalised drug delivery in cancer therapy, J. Controlled Release 370 (2024) 721–746, doi:10.1016/j.jconrel.2024.05.004.
[291] J.S. Tan, D.E. Butterfield, C.L. Voycheck, K.D. Caldwell, J.T. Li, Surface modification of nanoparticles by PEO/PPO block copolymers to minimize interactions with blood components and prolong blood circulation in rats, Biomaterials 14 (11) (1993) 823–833, doi:10.1016/0142-9612(93)90004-L.
[292] S.A. Kulkarni, S.-S. Feng, Effects of surface modification on delivery efficiency of biodegradable nanoparticles across the blood–brain barrier, Nanomedicine (2011), doi:10.2217/nnm.10.131.
[293] N. McDannold, N. Vykhodtseva, K. Hynynen, Blood-brain barrier disruption induced by focused ultrasound and circulating preformed microbubbles appears to be characterized by the mechanical index, Ultrasound Med. Biol. 34 (5) (2008) 834–840, doi:10.1016/j.ultrasmedbio.2007.10.016.
[294] M.J. Oldfield, C. Burrows, J. Kerl, L. Frasson, T. Parittotokkaporn, F. Beyrau, F. Rodriguez y. Baena, Highly resolved strain imaging during needle insertion: Results with a novel biologically inspired device, J. Mech. Behav. Biomed. Mater. 30 (2014) 50–60, doi:10.1016/j.jmbbm.2013.10.016.
[295] T. Watts, R. Secoli, F.R.y. Baena, A mechanics-based model for 3-D steering of programmable bevel-tip needles, IEEE Trans. Rob. 35 (2) (2018) 371–386, doi:10.1109/TRO.2018.2879584.
[296] M. Pinzi, S. Galvan, F. Rodriguez y. Baena, The Adaptive Hermite Fractal Tree (AHFT): a novel surgical 3D path planning approach with curvature and heading constraints, Int. J. CARS 14 (4) (2019) 659–670, doi:10.1007/s11548-019-01923-3.
[297] M.R. Dreher, W. Liu, C.R. Michelich, M.W. Dewhirst, F. Yuan, A. Chilkoti, Tumor vascular permeability, accumulation, and penetration of macromolecular drug carriers, J. Natl. Cancer Inst. 98 (5) (2006) 335–344, doi:10.1093/jnci/djj070.
[298] R. Raghavan, M.L. Brady, M.I. Rodríguez-Ponce, A. Hartlep, C. Pedain, J.H. Sampson, Convection-enhanced delivery of therapeutics for brain disease, and its optimization, Neurosurg. Focus 20 (4) (2006) E12, doi:10.3171/foc.2006.20.4.7.
[299] T. Yuan, L. Shen, D. Dini, Porosity-permeability tensor relationship of closely and randomly packed fibrous biomaterials and biological tissues: application to the brain white matter, bioRxiv (2023), doi:10.1101/2023.01.14.524065.2023.01.14.524065
[300] T.J. Lohela, T.O. Lilius, M. Nedergaard, The glymphatic system: implications for drugs for central nervous system diseases, Nat. Rev. Drug Discov. 21 (2022) 763–779, doi:10.1038/s41573-022-00500-9.
[301] M.J. Fowler, J.D. Cotter, B.E. Knight, E.M. Sevick-Muraca, D.I. Sandberg, R.W. Sirianni, Intrathecal drug delivery in the era of nanomedicine, Adv. Drug Deliv. Rev. 165-166 (2020) 77–95, doi:10.1016/j.addr.2020.02.006.
[302] W. Duch, K. Swaminathan, J. Meller, Artificial intelligence approaches for rational drug design and discovery, Curr. Pharm. Des. 13 (14) (2007) 1497–1508, doi:10.2174/138161207780765954.
[303] R. Gupta, D. Srivastava, M. Sahu, S. Tiwari, R.K. Ambasta, P. Kumar, Artificial intelligence to deep learning: machine intelligence approach for drug discovery, Mol. Diversity 25 (3) (2021) 1315–1360, doi:10.1007/s11030-021-10217-3.
[304] C. Meaney, S. Das, E. Colak, M. Kohandel, Deep learning characterization of brain tumours with diffusion weighted imaging, J. Theor. Biol. 557 (2023) 111342, doi:10.1016/j.jtbi.2022.111342.
[305] R. Padmanabhan, N. Meskin, W.M. Haddad, Reinforcement learning-based control of drug dosing for cancer chemotherapy treatment, Math. Biosci. 293 (2017) 11–20, doi:10.1016/j.mbs.2017.08.004.
[306] H. Mashayekhi, M. Nazari, F. Jafarinejad, N. Meskin, Deep reinforcement learning-based control of chemo-drug dose in cancer treatment, Comput. Methods Programs Biomed. 243 (2024) 107884, doi:10.1016/j.cmpb.2023.107884.